MATERIAL DESIGN METHODOLOGY FOR STRUCTURAL AND MICROWAVE MULTIFUNCTIONAL COMPOSITE LAMINATE SYSTEMS

by

Raymond McCauley

A thesis submitted to the Faculty of the University of Delaware in partial fulfillment of the requirements for the degree of Master of Science in Mechanical Engineering

Fall 2013

MATERIAL DESIGN METHODOLOGY FOR STRUCTURAL AND MICROWAVE MULTIFUNCTIONAL COMPOSITE LAMINATE SYSTEMS

by

Raymond McCauley

Approved: ____

Michael Keefe, Ph.D.
Co-Advisor in charge of thesis on behalf of the Advisory Committee

Approved: ____

Shridhar Yarlagadda, Ph.D.
Co-Advisor in charge of thesis on behalf of the Advisory Committee

Approved: ____

Suresh G. Advani, Ph.D.
Chair of the Department of Mechanical Engineering

Approved: ____

Babatunde A. Ogunnaike, Ph.D.
Dean of the College of Engineering

Approved: ____

James G. Richards, Ph.D.
Vice Provost for Graduate and Professional Education

ACKNOWLEDGMENTS

I would like to thank you to my advisors who have been excellent in giving me direction and advice in my work at the Center for Composite Materials.

Support provided by the Office of Naval Research (ONR) under grant N00014-10-1-0325. Electromagnetic modeling and measurements made by PhD candidate Peter Pa at University of Delaware, Department of Electrical and Computer Engineering. Further electrical insight advised from Mark Mirotznik, also Department of Electrical and Computer Engineering.

To my family and relatives who inspired me in pursuing my career in engineering. Especially my grandfather, Virgil McDonald , as without his guidance and early involvement, I would not be where I am today.

TABLE OF CONTENTS

Appendix

LIST OF TABLES

LIST OF FIGURES

ABSTRACT

Composite multifunctional materials are one way of hybridizing two material functions into one. One such application is in composite structures with electromagnetic (EM) functionality. Independently, mechanical and EM design methodologies exist, but there are limited design methodologies for making systems that combine both functionalities.

This research focuses on a design methodology for material selection involving a laminate-composite system with both structural and electromagnetic functionalities. One such application is for antenna radomes and composite deckhouses of naval structures that protect microwave equipment from external loads as well as provide electromagnetic functionality. These are typically sandwich structures which are optimized for high stiffness and low weight. This work shows, through systematic testing and characterization of failure, that the inclusion of an electromagnetically tuned layer in this system does not adversely affect the mechanical properties. Design and fabrication can be done with appropriate consideration of both regimes to produce a multifunctional material that is structurally sound and electromagnetically functional.

Chapter 1

INTRODUCTION

Multifunctional materials offer a means of hybridizing two or more performance regimes into one material with the added functionality of both into a single system. Particular attention has been devoted to structural materials with electromagnetic (EM) functionality. Currently, the design of composite sandwich structures [1] [2] [3] [4]and their mechanical characterization [1] [4] is well studied. The design of EM functionalized materials is also a mature field. Embedding layers within the laminate material imparts electromagnetic functionality, allowing it to behave differently when exposed to microwave radiation [6] [7] [8]. Although standards exist to separately design and test the structural and electrical [8] aspects of laminates, there are few design methodologies combining the two. This research provides a design and testing methodology to aid in a material selection for a certain class of laminate-composite structures by demonstrating that, for the system studied, the addition of an EM functionalized layer within the composite does not seriously degrade the structural performance.

1.1 Multifunctional Composite Materials with Radio Frequency Functionality Applications

Composite materials are commonly used in high strength, low weight applications. Their various weaves and fiber alignments can be tailored to generate the desired mechanical properties for the given application. Such applications include radomes and deckhouses for naval structures. Another benefit over traditional metal materials for naval structures is that composite materials consisting of fiber-reinforced plastic laminates do not suffer corrosion in the marine environment as quickly or as aggressively as do traditional metal materials. This could translate to less maintenance on these structures and further motivate the use of composites for naval structures.

1.2 Frequency Selective Surfaces

Multifunctional composite materials with electromagnetic functionality can be made with the addition of various conductive layers within the laminate. Electrical pathways can operate much like circuits to provide active sensing and embedded electronics. Other applications are passive, giving composite panels a unique electromagnetic profile over the microwave spectrum. An example of a passive application is a Frequency Selective Surfaces (FSS) which can be tuned to filter out specific frequencies by use of periodic conductive patches. Figure 1.1 shows an example of this surface including an embedded conductive pattern. When intercepted by electromagnetic waves, the conductive patches obtain a minute electrical current. This induces a polarity to the patches that resonates depending on the frequency of the wave. Patch geometry and spacing can be varied to tune this resonant frequency where the patches behave more like a ground plane and can reflect incoming electromagnetic waves [5]. How well this is done depends on patch shape as well as its size and periodicity. The included research can be applied to a wide range of FSS designs and tuned frequencies. The theory for predicting the electromagnetic response of these surfaces is well known and a variety of computer modeling programs are available [5] [9]. Research in this field stems mostly from traditional methods using Printed Circuit Boards (PCB). However these methods are typically not well optimized for structural properties. A greater emphasis on the structural regime is critical when designing these multifunctional systems that must be able to function electromagnetically as well as structurally.

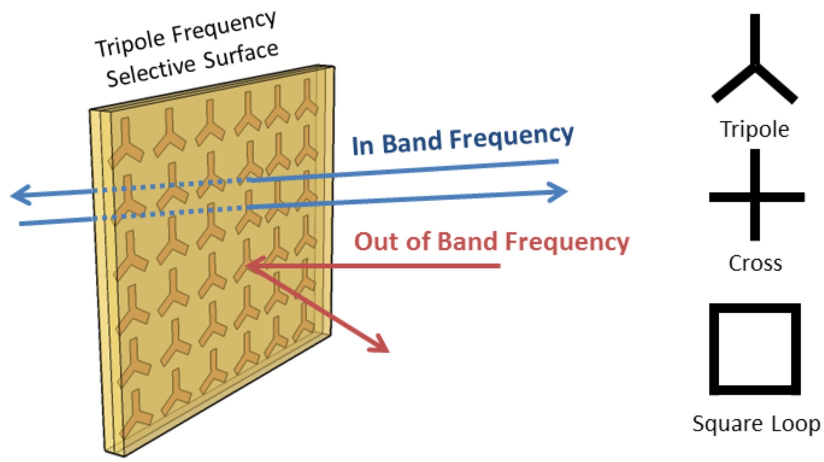

Figure 1.1: Frequency Selective Surface with Examples Patterns

Materials, such as the glass fiber reinforced composite materials, can be transparent to microwave signals and thus function well as radomes. Carefully designed composite materials allow the desired signals to reach antennas and radar equipment as well as protecting them against mechanical loads such as wind and blast loads from ship weapons. An example of this can be seen in Figure 1.2 showing a schematic of the mast of the USS Radford. Laminate construction allows the addition of layers that can be tuned to affect the transmittance of radio frequencies. High strength materials, coupled with unique EM signatures, can be used to make multifunctional composites to improve the efficiency of radomes.

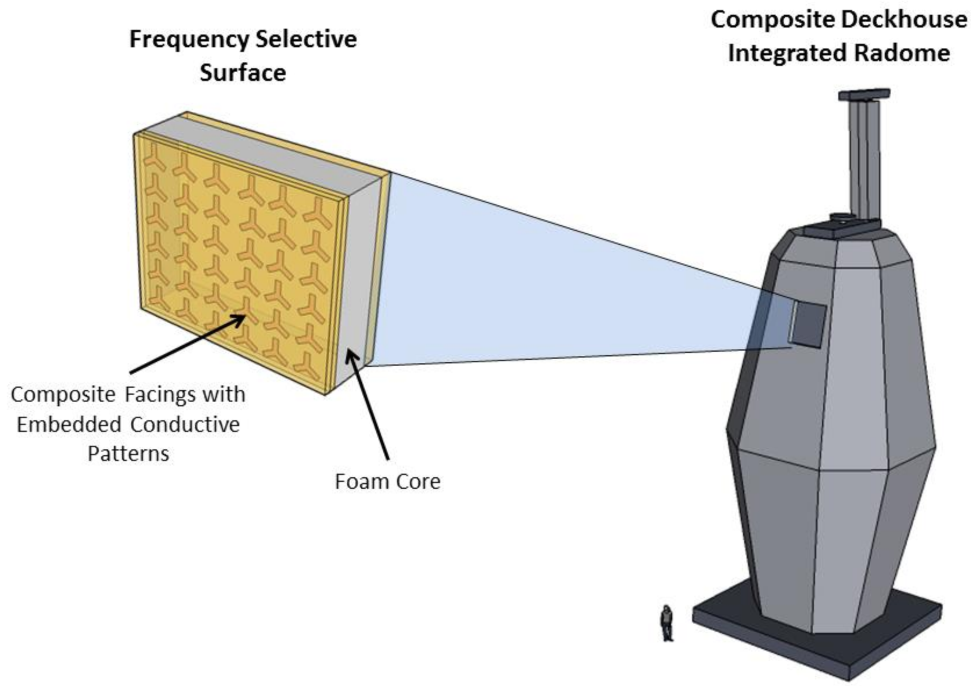

Figure 1.2: USS Radford Mast with Frequency Selective Sandwich Structure [1]

1.3 Structural Composite Laminates and Sandwich Structures

This work focuses on composite laminates that are used in making sandwich structures. Testing focus in this thesis relates to studying the adverse effects on the mechanical properties caused by embedding an FSS layer within the composite face sheets of a sandwich structure. Through characterizing the mechanical effect of including an electromagnetically functionalized substrate layer in the laminate-composite system, one can compare materials for selection. Investigating relevant mechanical effects caused by modifying various parameters of the PCB processing used to create the FSS material, should also give insight into failure modes.

Sandwich composite beams for structural applications are typically designed to be able to support high bending loads while being extremely light. How well they do this depends on the materials used as well as the geometry of the sandwich. Figure 1.3 shows a typical sandwich cross section loaded in bending. Here the face sheets are loaded in tension and compression while the core transfers the load to each using shear.   Adding an FSS layer will affect the material properties of the composite face sheets; thus the need to focus on face sheet mechanical properties. Tests first focus on adhesion between the composite laminate with added FSS materials versus the baseline without FSS materials. This leads into compressive and tensile properties which are used in predicting the sandwich structure's mechanical properties.

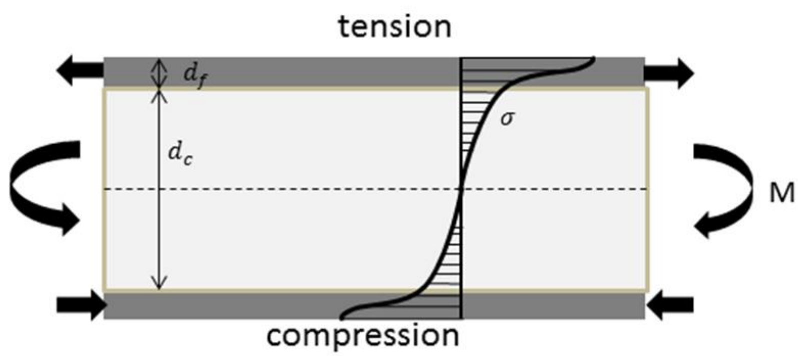

Important Properties

Face Sheets	E_f	σ_f	I
Core	E_c	σ_c	

Figure 1.3: Sandwich Beam in Bending

where:

E_f = face sheet modulus

E_c = core shear modulus

σ_f = face sheet strength

σ_c = core shear strength

I = area moment of inertia

1.4 Thesis Outline

This work discusses the material-selection design and testing of passive electromagnetic application, created by embedding an FSS within a composite laminate sandwich structure. In Chapter 2 both the mechanical and the electromagnetic regimes are investigated. Then work in relevant multifunctional design for composites is presented. A candidate FSS substrate layer is chosen in Chapter 3 and mechanical properties are inspected after the PCB processing used to make it into an FSS. Chapter 4 describes the actual laminate fabrication and testing with Chapter 5 focusing on summarizing the test results. Particular attention was paid to adhesion and shear testing to look at the bond between the substrate and the surrounding structural composite. Mechanical properties are measured comparing the baseline composite to a few substrate cases as well as a variety of FSS patch configurations. Chapter 6 describes how the data was used to make a multifunctional composite sandwich beam with test results compared to a purely composite baseline without an FSS layer. Chapter 7 summarizes the test data and shows that the inclusion of this particular FSS layer into the designed multifunctional system does not seriously degrade the structural performance. Understanding layer-to-layer adhesion can give much insight into how these substrates interact within a given composite system. This is critical for as a design methodology for this and other multifunctional laminate material systems.

Chapter 2

LITERATURE REVIEW AND PRIOR RESEARCH

Design of multifunctional composite materials stems from previous work in electrical design and structural composites. These two methodologies are well understood independently and there is extensive literature on their design. However, little work has been done hybridizing the two and providing a design methodology that results in little or no loss in mechanical and electromagnetic properties. Current research focus has been on simple model systems looking at specific applications or attributes in an attempt to characterize and measure electrical and structural properties.

2.1 Mechanical Design and Theory

Composite sandwich structures are a typical means of attaining high stiffness with reduced weight. The theory and methodology for the design and fabrication of composite sandwich panels is well developed [1] [3] [4] [10]. Yet some applications are not only mechanically driven but also electrically driven. Good examples of these are radomes for naval vessels which protect antennas and electrical hardware from wind and blast loads from ship artillery [11]. Structural radome design is well known but limited to radio transparent composite surfaces without embedded tuned EM layers. A design and testing methodology is necessary to effectively hybridize these design paradigms in order to more effectively make these multifunctional composite materials.

2.2 Electromagnetic Design and Current Approaches

Much of FSS work stems from traditional PCB board fabrication. The electromagnetic theory is mature for the design of these and fabrication methods are done with high consistency. Conductive pathways, or in this case patches, are made through etching away conductive copper layers [5]. Materials used in making PCB's are tuned specifically for EM response and are readily available in the market. Most designs are for flat boards with little concern for structural properties other than thermal loads due to heat dissipation of microchips [12].

Design criteria for electromagnetic properties depend on geometry and materials used. For geometry the patch shape can dictate how effective the FSS is at resonating with a given frequency. Patch size, spacing, and orientation are varied to tune the materials to specific frequencies. The patches must also be conductive and the dielectric properties of the surrounding composite known in order to make accurate models. The electromagnetic response for these can be predicted theoretically [5] [9] as well as simulated using Finite Element Analysis (FEA) software. Once such FEA software package for this is HFSS developed by Ansys® which is used for designing the FSS geometries studied in this work. Experimentally, the electromagnetic response of a board can be measured using an anechoic chamber capable of measuring transmittance as well as reflectance as seen in Figure 2.1. This is often used to confirm EM theory which is very sensitive to material properties and geometry.

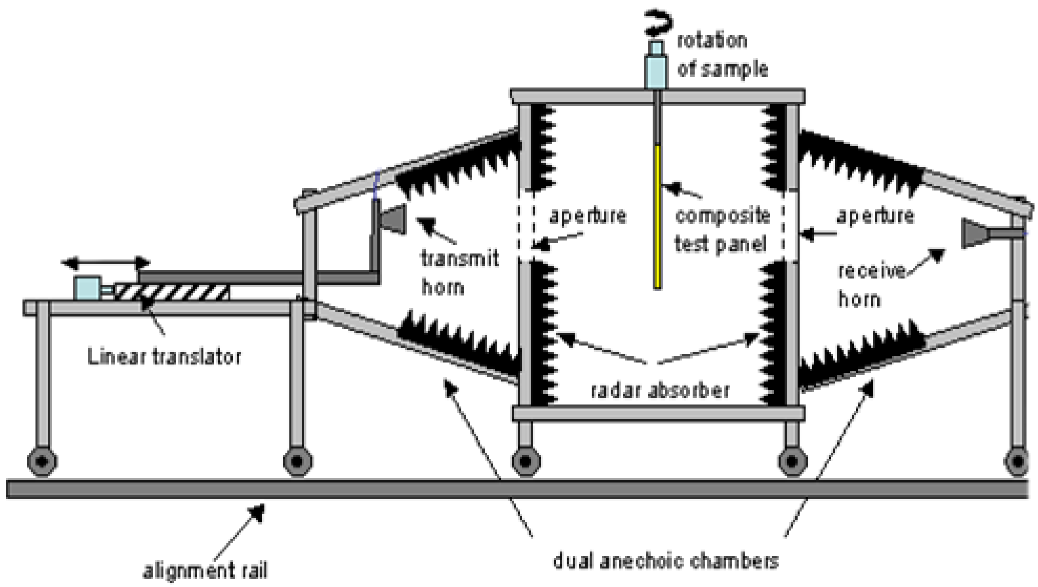

Figure 2.1: Dual Anechoic Chamber for Measuring Microwave Response with 30x30cm Composite Test Panel

2.3 Multifunctional Structural Composites with Electromagnetic Functionality

Conductive layers have been added to composite materials to give added electrical functionality. One such application has been for active sensing. Stanford University produced a SMART layer featuring the same conductive pathways and polymer film with piezo-electric sensors [13]. Here a flexible copper-clad Kapton was etched with the desired circuit and placed within the laminate stack. This material is commonly used in PCB fabrication. The composite laminate featured a prepreg system which was processed within autoclave conditions. Extensive tests were done to measure structural properties focusing on interlaminar strength including short beam shear, lap shear, and flatwise tension. These preliminary tests were done to look at bond effects before the actual SMART layer was tested in compression and tension.

It was found that there was no reduction in structural properties and that embedding surface treated layers slightly improved interlaminar properties. This emphasizes that attention to interlaminar bonding when adding these layers are critical to maintaining mechanical properties.

Additional active electromagnetic applications are antennas. These are extensively used by aircraft and vehicles for communication as well as sensory applications. With the weight reduction and improved strength that accompanies composite fabrication, a means of integrating antennas into composites have been developed. One such composite system is cyanate ester resin coupled with glass fiber reinforcement to produce a strong composite system that is low loss when placed in front of a radiating element such as an antenna [14]. Common mechanical failure is noted to be within the interlaminar region due to adhesion issues and stress concentrations from embedded materials. Structural design usually revolves around sandwich and multi-layered construction [15] [16]. Inner layers function structurally while outer, radio permeable, layers are coupled with antennas.

The core material, within a composite sandwich structure, is one such location to embed an electromagnetically tuned layer. Some guidelines for this design, from an EM standpoint, exist in literature although focus has only been on electrical design [17]. Choi designed a low-observable radome prototype with a microwave filter layer placed in the mid-plane of the sandwich within the core [18]. The filter was made from etched aluminum foil bonded to a polyimide film to filter out a specific microwave frequency. This layer was bonded to the foam core using an epoxy adhesive before adhering the composite face sheets which were made from either E-glass or aramid fiber reinforced epoxy prepreg. Mechanical testing focused on impact

(ASTM D7136). Sandwich panels were compared structurally as well as electromagnetically by comparing the microwave response of the panel before and after impact. Response was measured using antennas to find microwave transmittance and absorbance. Samples failed similar to the baseline composite and measurements focused more on the impact's effect on EM properties. Similar work was done with the electromagnetically tuned layer placed within the core-to-face sheet region with similar focus on testing impact effects [19].

Other than impact, composite sandwich structures are also loaded in bending during their lifetime. One such scenario added a nano-clay material to tailor dielectric properties [20]. Mechanical testing was done through 3-point bend. Strength was related to the amount of nano-clay used as well as a comparison of the baseline sandwich panel to the one with the added layer. Results found that the flexural strength does diminish with the addition of this specific electromagnetic material within the sandwich panel.

Conductive printable ink has been used to produce an FSS within structural composite material [21]. Periodic conductive patches were screen printed directly onto a composite glass prepreg before being placed within the composite stack and bagged for cure. The microwave response was measured before doing short beam shear testing (ASTM D2344). A slight decrease in properties was measured versus the pure composite baseline without the FSS pattern. Failure was observed as cracks and debonding within the embedded layer and the surrounding composite.

There has been some research focusing on the structural properties of copper foil patches placed within composite laminates [22]. These patches are analogous to FSS design although, in this case, were not arranged with EM properties in mind but rather mechanical properties. This study was done to observe the mechanical effects of having an embedded copper patch with various surface treatments. Here the laminate stack was made using Vacuum Assisted Resin Transfer Molding (VARTM) to infuse a vinyl ester resin into a woven E-glass stack containing the copper patches. The copper patches were placed midplane and a variety of tests were done including tension, compression, and flexural. Only a small reduction in modulus occurred but a large reduction in strength was observed. Strength reduction was most noticeable in compression and flexural testing. This can be related to the size of the patches as well as the surface treatment used on the copper relating directly to bond strength. Here, a strong correlation exists between how well the added material bonds, the size of the inclusion, and how it performs in strength.

Within composite loading regimes, the strain to failure of the composite is often much higher than that of the embedded conductive substrate. This becomes a concern as the loads the composite experiences in service can detrimentally deform a conductive substrate such as copper. This can lead to premature failure, both electrically and to the copper-to-composite bond. In one study, a glass fiber composite specimen contained an embedded electrical grade copper strip within the midplane [23]. Electrical contacts were placed on either end of the copper and the sample was tested in static failure as well as tensile cyclic loading. The sample was then loaded statically and failed in tension as well as cyclical loading at loads lower than failure load of the composite. For static loading, the composite failed first but the ductile copper stayed intact and maintained a conductive pathway. However, under cyclic loading, the copper failed first and caused debonding from the surrounding composite as well as cracks in the copper. This resulted in a loss of conductivity. Samples tested at 20% of the ultimate failure load saw no degradation in the copper although this underutilized the capabilities of the structural composite. Failure analysis was done through ultrasonic C-scans as well as electron microscopy. Debonding was easily observed as well as local cross-sectional area reduction at the copper cracks suggesting plastic deformation prior to failure.

Further integration into structural composites features conductive fiber reinforcement. Instead of including conductive layers between the fiber lamina, the conductive material is the fiber reinforcement itself [24]. Conductive fibers, such as carbon fibers and metal plated glass fibers, as well as carbon nanotubes [25] have been used. These materials have great potential in conformal antennas and EM structures as they can bend with the composite [26]. Fibers can be made conductive with metal plating and are used in conjunction with nonconductive fibers such as glass or Kevlar. The arrangement of the conductive fibers allows the composite to act as a filter for microwaves. Conductive fibers can also be used actively in the form of antennas [27] as an alternative to conductive foil substrates which have commonly failed in peel or delamination. These systems have been fabricated but are relatively new and little to no mechanical tests have been done.

2.4 Synopsis and Key Themes

The bulk of the previous research has focused more on design of specific electromagnetic properties, working from current PCB -based systems, and then simply checking structural performance as there is little desire for heightened mechanical properties. Current literature is more concerned with loads due to thermal stresses as well as the attachment of microchips [12]. Any models on the mechanical loads on PCB boards stem from laminate theory but anticipate loads much lower than those experienced in structural composites. In order to apply the same processing of PCB materials to structural composites, materials need to be reexamined in higher strength structural regimes.

It can be seen from literature that poor adhesion degrades shear properties as well as compression properties. This is critical for composite sandwich structures as loads often transfer through the composite lamina through shear. The face sheets of the sandwich structure also experience tension and compressive loads when the sandwich experiences bending loads. These loading regimes are rarely studied in PCB materials and must be revisited for structural composites. Through focusing on these mechanical effects, one can develop a design methodology appropriate for both EM and structural regimes. This motivates a hybrid approach stemming from both PCB and mechanical design approaches.

Materials used in this research stems from both structural composites and PCB materials. The composite system must be non-conductive and allow microwave radiation to pass freely. This motivates the use of glass fiber reinforced composites with low loss resins systems such as cyanate ester. Conductive substrates must also be chosen. Copper-clad films are commonly used in multilayer PCB boards and are made to be easily etched and bonded to surrounding lamina. As seen from the literature, copper-clad Kapton films are commonly used in fabricating electromagnetically functional layers. Mechanical adhesion of the EM layer to the surrounding composite layers greatly depends on surface treatment and processing of the film and foil substrates. Since the core in a multifunctional composite sandwich structure must have low loss in the electromagnetic regime, this motivates the use of a honeycomb structure; this type of core material is commonly used in aircraft structures featuring antennas and radomes.

Chapter 3

MATERIALS AND PROCESSING

Design of multifunctional structures starts with materials that must satisfy both structural and electromagnetic requirements. A variety of materials exist for use in structural composites as well as PCB boards. The approach in this work focuses on one such suitable composite system and PCB material.

3.1 Baseline Structural Composite Materials

Composite material selection was driven by design requirements, both electrical and mechanical. The prepreg system chosen for this research was the Tencate™ BTCy-1 featuring a cyanate ester resin and a 6781 8-harness satin S-glass woven fabric. This system performs well structurally and is designed for use in radomes [28]. This system is preimpregnated with resin and thus does not require resin infusion. This is beneficial as the FSS layer used is impermeable to resin flow and would interfere with infusing the dry fiber. Prepregs can also be processed within autoclaves where the high pressures can minimize the size of any voids that may occur within the part.

To be utilized for electrical applications, the composite system must also have an established dielectric constant and low loss. Each material has its own dielectric property which can affect the electromagnetic response of the designed FSS. Loss refers to the signal strength lost as an electromagnetic wave passes through the material due to impedance mismatch and signal reflection. Fiber Volume Fraction

(FVF) content is also a concern as varying percentages of resin to fiber content can change the dielectric constant. This has been seen in EM measurements and models have been adapted to feature fiber volume fraction to calculate dielectric properties [5], [29]. Autoclave processing assists in keeping the FVF and in turn the mechanical properties and dielectric properties consistent.

3.2 Frequency Selective Surface Materials and Relevant Substrates

The substrate on which the FSS is made must serve various purposes. As mentioned before, it provides conductive patches which are electrically isolated from each other and thus tuned to the desired microwave frequency. They must also be fixed relative to each other and maintain a constant spacing. Finally, the substrate needs to show good structural properties and not be mechanically isolated from the surrounding composite. Industry offers many materials that fit this criteria and the material chosen for this work is described in the following sections.

3.2.1 Substrate and Material Selection for Electromagnetically Functionalized Layers

In order to tune and give electromagnetic functionality, the material needs a conductive layer or patches of a conductive material. There are a variety of metals available with good electrical conductivity. Traditional PCB fabrication uses copper foil due to ease of etching and surface treatments. This material is extremely conductive and readily available. Copper foil comes on a variety of substrates including polymer films.

In order to be properly etched the copper must be bonded to another substrate. This fixes the patches in position relative to each other. For this purpose standard polyimide film Kapton bonded to a copper foil was used. Dupont® produces a system known as Pyralux™ which also features treatment to improve bonding for both the copper as well as the Kapton. The Pyralux™ LF9110D was chosen for this research and consists of a 28.4 gram (1 oz.) weight copper bonded to $2.54 * 10^{-3}$ cm (1 mil.) thick Kapton. The copper is electrodeposited to produce a roughened surface, increasing surface area and allowing it to adhere well mechanically to most adhesives and resins. The Kapton surface is corona treated by use of plasma to improve surface activation energy shown to provide excellent chemical adhesion.

Before working with the actual Pyralux® film, an assessment was made of the constituent materials. This included copper and Kapton without the surface treatments for adhesion. For this, a 1oz. copper foil made by Oak Mitsui was chosen featuring a drum side with lower surface roughness, as well as a matte finish side with higher surface roughness. This copper foil system is marketed for applications where adhesion is not a concern for one of the surfaces. Kapton film made by Richmond Aircraft Products®, model UHT-750, was used as the untreated Kapton variant. Oak Mitsui also makes a treated copper foil, DBT-III, similar to the copper featured on the Pyralux®. Dupont™ also makes a corona treated Kapton, FPC200, which is the same Kapton film used in the Pyralux™. From these baseline materials, bond properties can be assessed working from the ground up emphasizing surface treatments. Figure 3.1 lists the material testing steps used in this work, proceeding from the baseline pure materials to those used in the FSS layer.

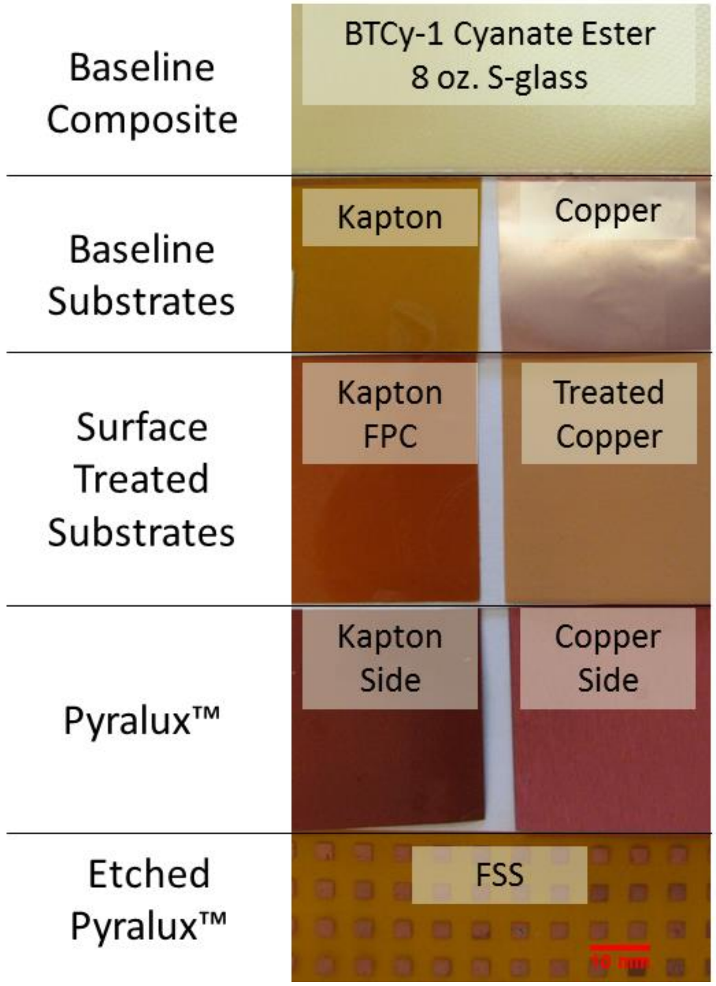

Figure 3.1: Constituent Material Design and Testing Flow Working Down From Baseline Composite, the Pyralux™ Constituent Materials, and the Full FSS

3.2.2 Frequency Selective Surface Patch Selection and Design

Design criteria for electrical properties depend on geometry and materials used. Patch size, spacing, and orientation can be tuned to specific microwave frequencies. The patches must also be conductive and the dielectric properties of the composite known in order to make accurate models. Electromagnetic properties are taken into account during material selection as well as measured in the anechoic chamber for use in modeling.

The effect of the FSS pattern chosen on the mechanical properties needs to be easily tested, and the FSS pattern chosen needs to be measured electrically within a relevant microwave frequency range. Solid square patches function well as an FSS and are geometrically orthogonal as is the woven glass reinforcement of the composite. The sizes of the patch and spacing also are suited for K-band microwave signals. A simulation sweep was done varying the patch sizes and spacings. This was done using the Finite Element Analysis software HFSS at the University of Delaware Department of Electrical and Computer Engineering. The quality as an FSS was then determined based on the ability to filter out a measurable frequency as well as having low loss when out of frequency. Representative patch geometries were then chosen to be fabricated and tested. This procedure is outlined in Figure 3.2.

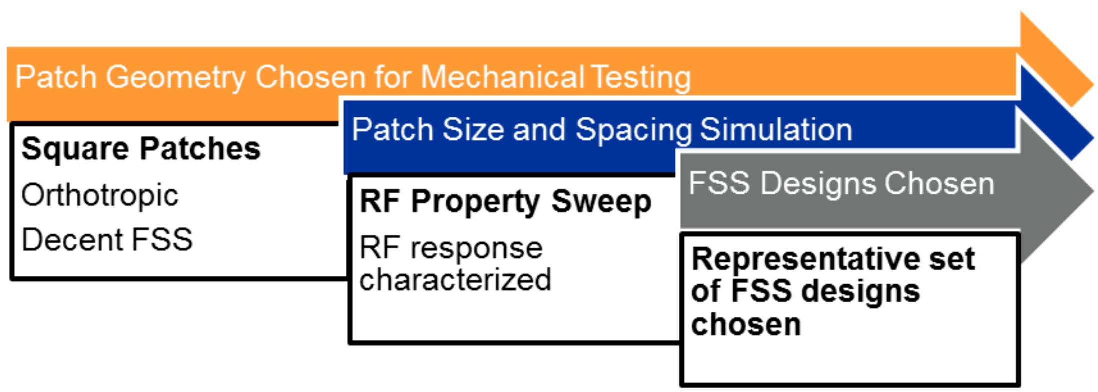

Figure 3.2: Frequency Selective Surface Design Flow

Processing for the Pyralux® film to make an FSS layer followed standard industry practices for PCB materials. This was outsourced to Fineline Circuits Inc. who specialize in PCB etching. First the copper side of the film was coated with a photoresist. This photoresist reacts when exposed to UV light and then can be dissolved off. A transparent filter with the FSS design in opaque ink was placed over the photoresist allowed only the light to reach portions of the resist to be removed. Once this was completed the film was placed in an etchant solution that easily dissolves copper. Here the copper not covered by the resist was removed leaving only the copper for the FSS design behind. Remaining resist was then removed leaving behind the complete FSS film. Diagrams for this methodology can be seen in Figure 3.3. The FSS layer was then placed within composite laminate stacks and cured under autoclave pressure. Final manufactured samples are shown in Figure 3.4 featuring the FSS layer, FSS embedded in multilayer composite, and final sandwich structure.

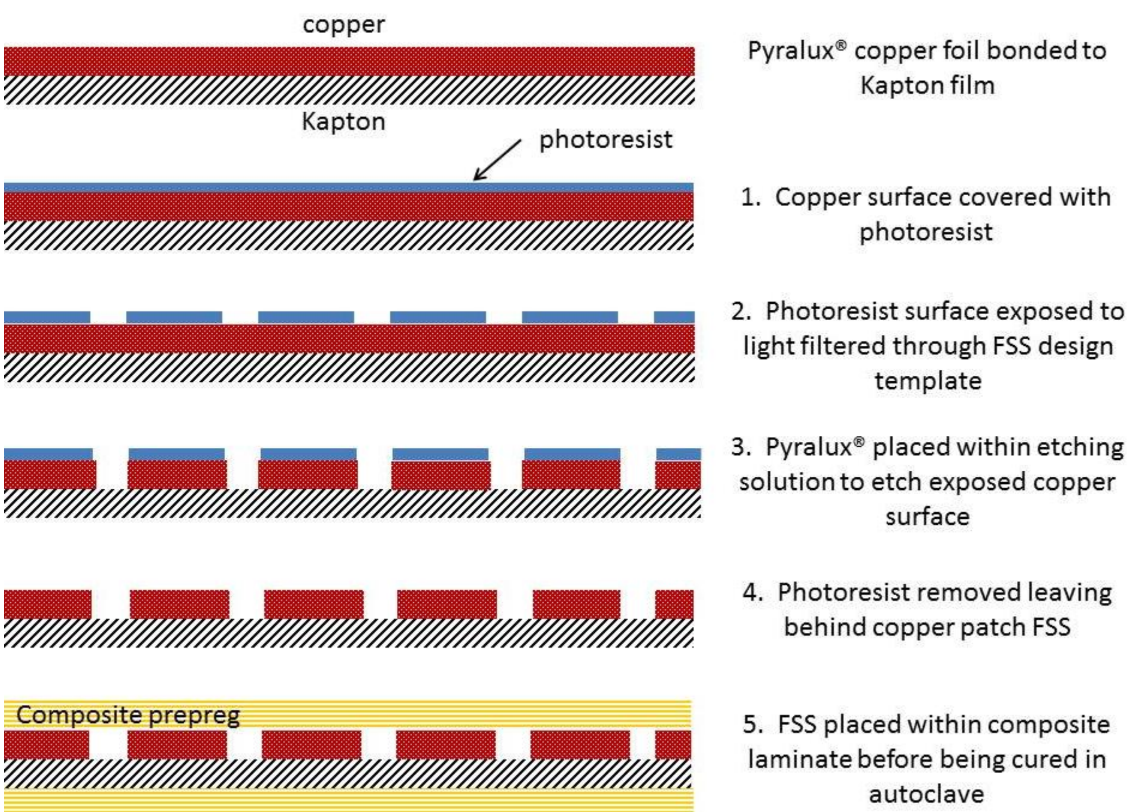

Figure 3.3: FSS Etching Procedure

Geometric design for the FSS was split into two parameters; the size of the patches and how they were spaced within the gage section. For these tests 2, 3, and 4 mm patch sizes were selected. Spacing was designated by the largest unit cell which fit within the 2.54 cm (1 inch) gage section to be used in mechanical tests. Spacings chosen allow for the thickness of the diamond saw blade used to cut the composite. This makes sure that the patches are aligned with the samples and are the same distance from the cut edges after each sample is cut. Each patch size and spacing scenario was modeled using HFSS™ to predict the EM properties and how well it operates as an FSS. The data for this is available in the Appendix. Some of the scenarios were also selected so that they would both have the same area of copper but represent different sizes and spacing of patches.

The final FSS designs were tested and used in a composite sandwich design. Having two face sheets means there can be two FSS surfaces making the sandwich stack symmetric. In electrical applications, one can use two different FSS's to be able to filter out two frequencies [5]. Here the FSS was placed within the midplane of each face sheet. Two layer face sheets were chosen because they could contain the FSS layer within the midplane as well as fail at a lower load then the chosen core material. The core must also be low loss, motivating the choice of a honeycomb core which was measured in the anechoic chamber. Figure 3.4 shows the final etched FSS layer as well as composite panels with the layer embedded.

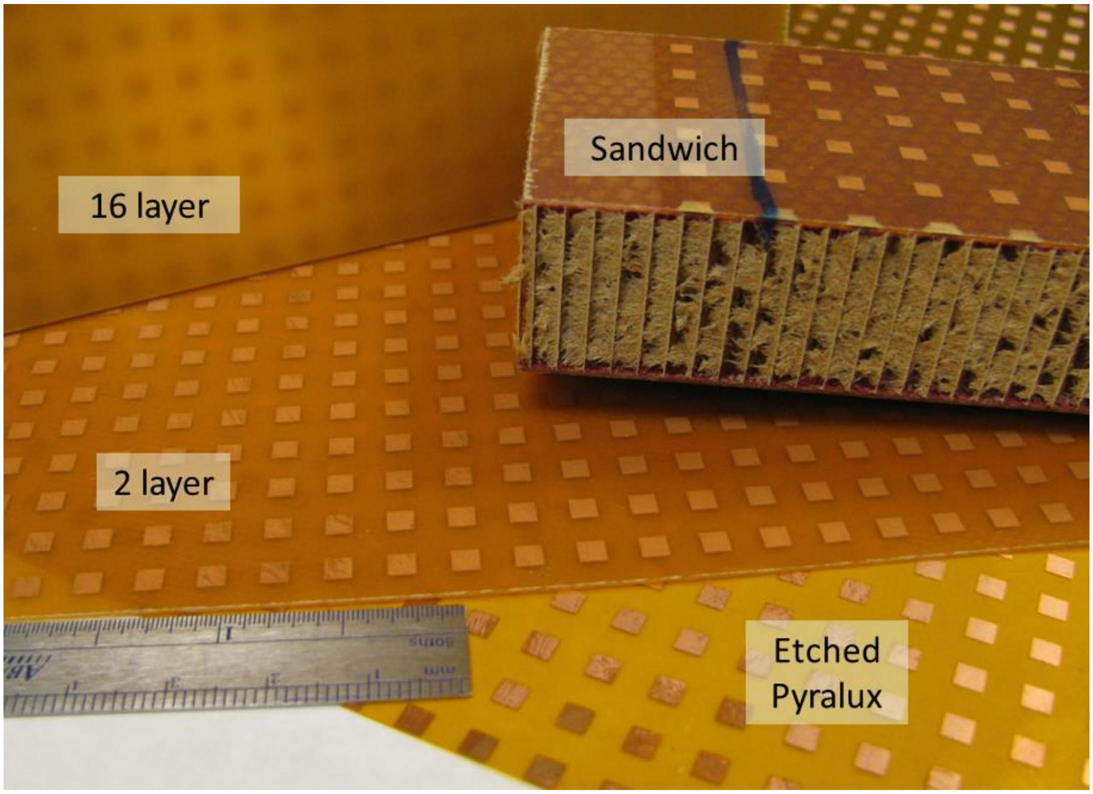

Figure 3.4: Etched FSS layer, Composite Test Materials, and Final FSS Sandwich

Chapter 4

LAMINATE SAMPLE FABRICATION AND TESTING PREPARATION

Composite fabrication and handling followed procedures specified by the material supplier. All properties were measured in the warp direction of the fiber and plies were flipped to make each composite panel midplane symmetric. Composite samples, featuring EM substrate layers, proceeded from the pure composite baseline testing. Due to the laminate construction of PCB materials, the EM substrates were added to the composite stack within the interlaminar regions.

4.1 Baseline Composite Processing

Composite processing for this research followed the standard procedures on the datasheet supplied by Tencate® [30]. The prepreg was handled and cut to size after reaching room temperature to eliminate water condensation on the prepreg surface. Laminate stacks were consolidated using a roller to remove large air pockets. It is at this stage that the electromagnetically functionalized substrate to be tested was placed within the lamina. Since the 6781 8 harness satin weave is not balanced, the warp and weft directions were aligned for each lamina. Plies were also flipped about the mid-plane of the complete stack to prevent any warping that could be caused from asymmetry. Mechanical testing focused on properties in the warp direction for consistency. For the thick panels, every 8 layers of the prepreg were debulked under vacuum before being combined into the complete laminate stacks.

Processing for cure featured elevated temperature and pressure from an autoclave made by Thermal Equipment Corporation (TEC). On the the autoclave table surface was placed a release film before laying up the prepreg layers. Once the composite prepreg was placed, another layer of release film was used to cover the entire part followed by glass fiber tows placed at each corner of the prepreg to allow air flow out of the release film pocket. To produce a smooth and consistent surface finish, 1.27 cm (0.5 inch) thick aluminum caul plates are placed over the top layer of release film. A layer of polyester breather fabric was placed over the entire part to allow a pressure differential between the autoclave environment and the part below. This breather was in contact with the vacuum line, pressure transducer, and the glass tows at the corners for full vacuum flow. A diagram of the bagging procedure can be seen in Figure 4.1 as well as the actual layup before adding the bagging film. Once this was completed the vacuum bag was placed over the entire part before being leak-checked.

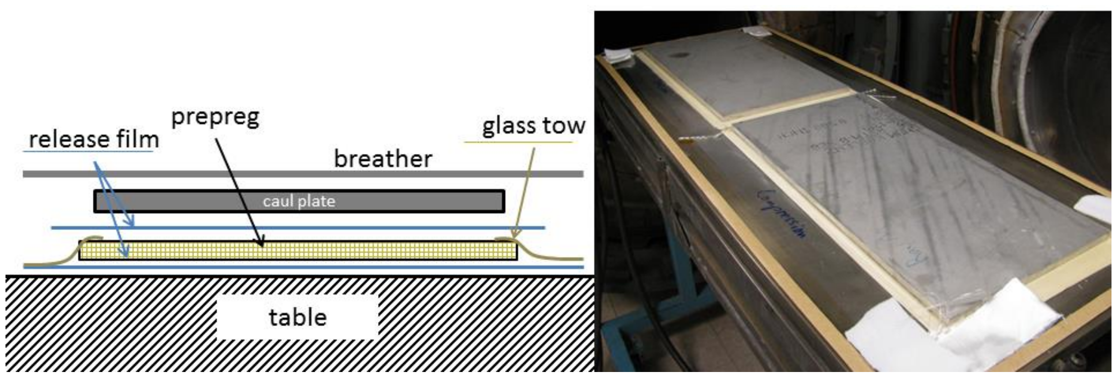

Figure 4.1: Layup and Bagging Featuring 1.25cm (0.5 inch) Thick Caul Plates

The autoclave run follows the cycle shown in Figure 4.2. Once leak-checked, the part was sealed and pressure ramp up began using nitrogen gas. Full pressure of

344 kPa (50 psi) was reached before bringing temperature up to 176.7 °C (350°F). A thermocouple measured and logged the temperature of the part directly. Vacuum to the part was applied for the duration of the run. Following a 90 minute dwell to cure, the temperature is brought to 71 °C (160°F) before pressure was released. All parts were allowed to cool before being removed and processed for testing.

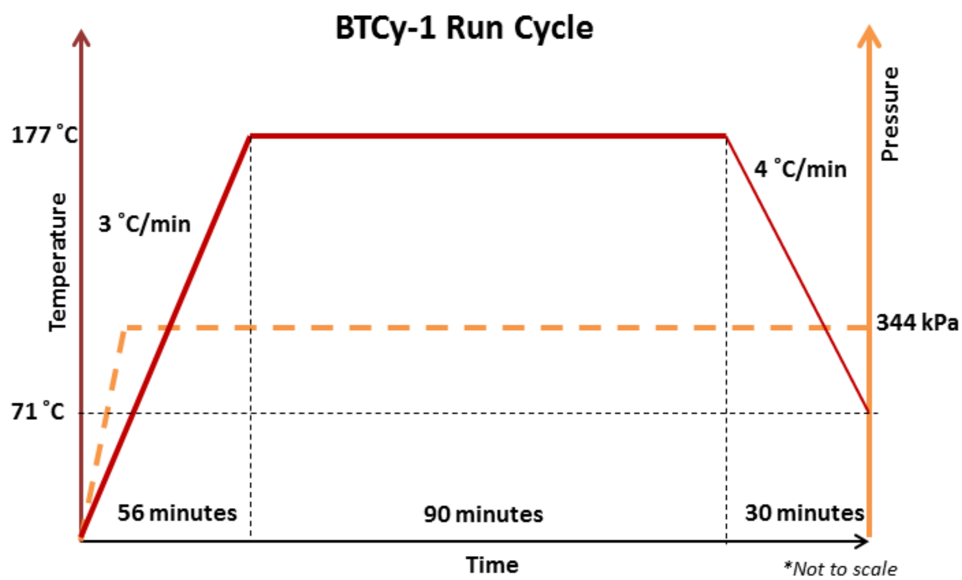

Figure 4.2: Prepreg Run Cycle

4.2 Substrates, Frequency Selective Surface Design, and Processing

Electromagnetic substrates tested were placed within the composite laminates at specific locations based on FSS design. These came in the form of films and foils which were easily placed between the prepreg layers. Care was taken to preserve surface cleanliness before being applied to the composite prepreg. In the case of bi-layered substrates such as the Pyralux™, care had to be taken to differentiate the copper side from the Kapton side. This was most important to adhesion testing as failure initiation and orientation of the test sample for these bi-layered substrates affected mechanical properties and failure location.

The FSS designs in this study were primarily made with the objective of mechanical testing although design had to start with electromagnetic performance as the motivation. Square patch patterns were chosen since they are geometrically orthotropic and perform moderately well in the K-band [5]. Patch sizes and spacing were driven by the ASTM standards to give a good range of scenarios while keeping patch location in the gage length consistent. The spacing between patches was chosen to account for the blade width used for cutting the samples. After each cut there would be the same number and alignment of patches in each sample. For a 0.18 cm (0.07 inch) diamond wet-saw this accounted for spacings of 13.59, 9.07, 6.79, and 5.44 millimeters. A schematic of the geometry can be seen in Figure 4.3. This geometry both satisfies the requirement of the mechanical testing standard as well as the frequency range in which we are interested. The K-band ranges from 12-40 Ghz and corresponds to a wavelength that is small enough to be measured within the lab through use of an anechoic chamber.

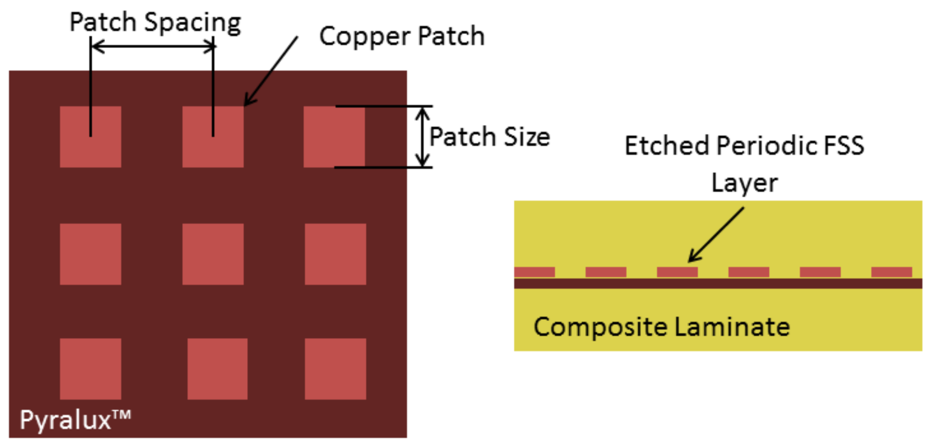

Figure 4.3: FSS Square Patch Geometry

Once the patch sizes and spacing were chosen, they were analyzed using the simulation software HFSS which was used to predict the quality of the FSSs and their resonant frequencies. These are later confirmed with measured results from an anechoic chamber. The anechoic chamber contains two antennas which can be focused and used to measure transmitted waves and reflected waves. The distance of the antennas limits the frequency range of which can be measured thus the FSS designs were chosen to fit within the K-band range, 12-40 GHz. This means of testing and verification is non-destructive and was done before sample preparation and cutting.[1]

[1] Electromagnetic simulation work and testing done in conjunction with Peter Pa, University of Delaware Electrical and Computer Engineering Department.

4.3 Testing Methods and Setup

Testing of these multifunctional materials was both electromagnetic and mechanical. Microwave testing and measurement is nondestructive and was done before mechanical tests. The mechanical tests failed the samples completely to find structural properties both in the elastic and failure regime. This methodology allowed the use of the same sample for both testing regimes.

Test sample preparation of the composite panels is as follows: first excess resin and fabric were cut from the edges of samples using a diamond-bladed wet saw. Thickness measurements and weights of each panel were recorded. An ultrasonic C-scan was performed to check for any large voids or inconsistencies in the composite. The panels were immersed in water and scanned with a 5 MHz transducer. An example of this can be seen in Figure 4.4 showing a panel with a wrinkle in the embedded copper film beside a proper panel. Wrinkles were uncommon and samples were cut from locations in the panel devoid of such blemishes. These cuts were aligned with the fiber warp direction as best as possible keeping lines parallel with the factory edge of the pepreg roll. Additional samples were cut and used for measuring fiber content via burn-off testing. This was done in accordance to standards that measured FVF, ASTM D2584 [31], and void content, ASTM D2734 [32].

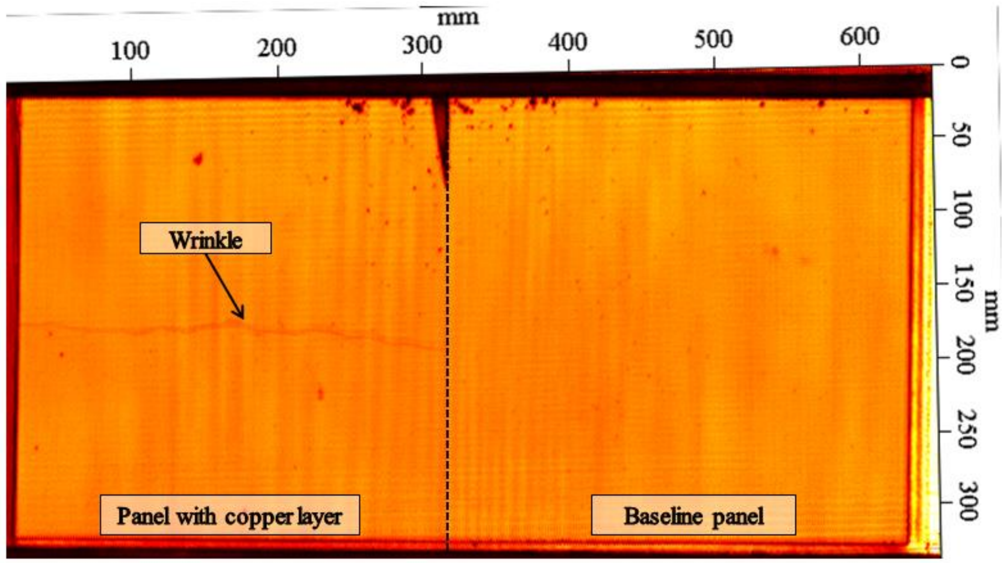

Figure 4.4: Example C-scanned Panels

The testing scheme and order for component testing can be found in Figure 4.5. The process of material selection by looking at bonding helps reduce the number of mechanical tests that need to be done later. In this research, these tests were used to characterize the chosen system of Pyralux™ as much as possible before it was sent out to be etched into the FSS. Once good bond strength was confirmed, tests continued into the mechanical regime ultimately used to predict the mechanical properties, modulus and strength, of a composite sandwich structure.

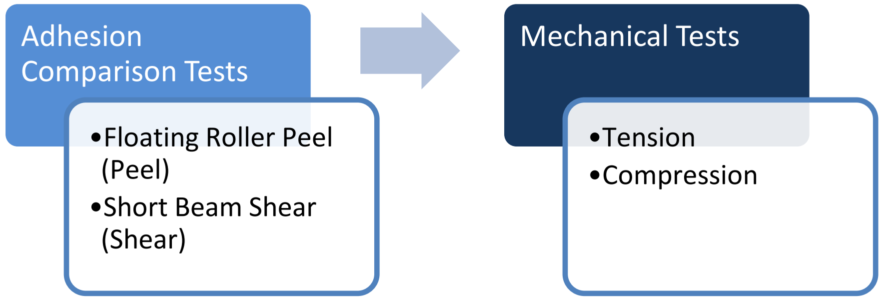

Figure 4.5: Testing Scheme; First Comparing Adhesion and Shear Failure before Characterizing Mechanical Properties

4.3.1 Adhesion Comparison Testing

For mechanical properties, interest was focused on what the effect the FSS will have on the surrounding composite layers. Initial focus was on substrate adhesion in peel and shear compared to the pure composite baseline. Bonding is the means through which the FSS layer interacted with the surrounding composite. For this, peel and shear failure were of most interest. Figure 4.6 shows the potential modes with the failure bond surfaces in red. Bond properties were compared for baseline composite and the composite with added FSS materials. Floating roller peel testing was chosen as a comparative means of measuring bond strength and locating failure interfaces following ASTM D3167 [33]. In addition, ASTM D2344 [30], was used to compare short beam shear strength of the composite with the embedded substrates and FSS layer. These tests function as preliminary tests to compare materials used as well as give insight on where failure may occur in the laminate.

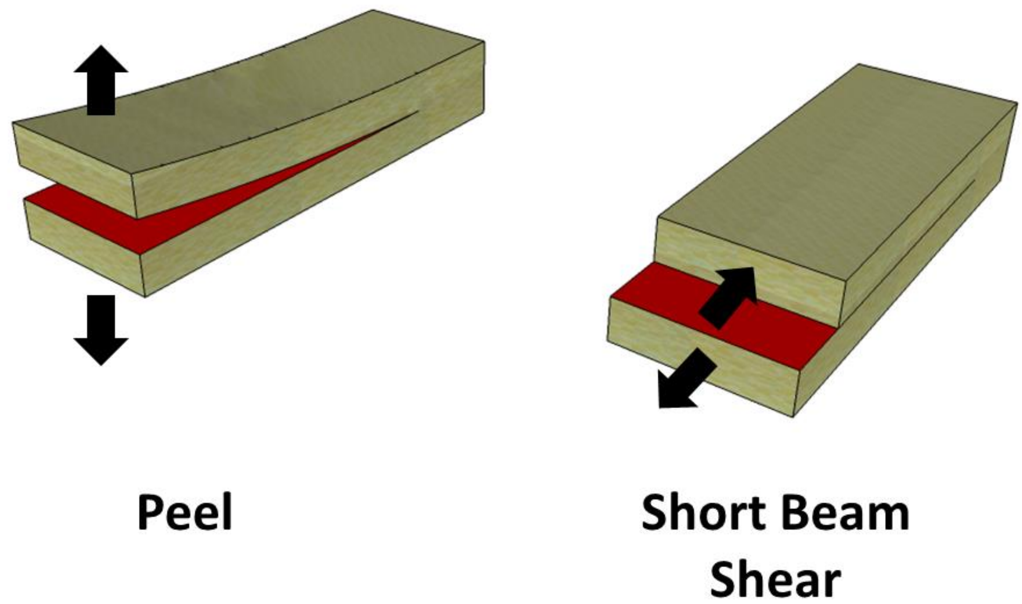

Figure 4.6: Interlaminar Failure Modes with Failure Surface Shown in Red

4.3.1.1 Floating Roller Peel Sample Fabrication and Testing Description

Floating Roller Peel (FRP) samples were made to compare bond strength and investigate failure mechanisms in the chosen materials in accordance with ASTM standard D3167 [33]. These were fabricated from 8 layer stacks where the material in question was placed between the 7th and 8th layers. Release film was placed between the 8th layer of the composite and the embedded material. This film extended at least 7.3 cm (3 inches) into the sample as a pre-crack so that the testing fixture could differentiate and peel the two layers apart. Individual specimens were cut to widths of 1.27 cm (0.5 inch) per ASTM standard instructions. The samples were labeled and the widths measured in three different locations along the sample. These widths were averaged and compared to the peel strength to derive the strength per unit width of peel. Testing was done using an Instron® 5565 with a 500 newton load cell which was first calibrated using a known weight. Figure 4.7 shows the 1.27 cm (0.5 inch) wide peel sample loaded within the test fixture.

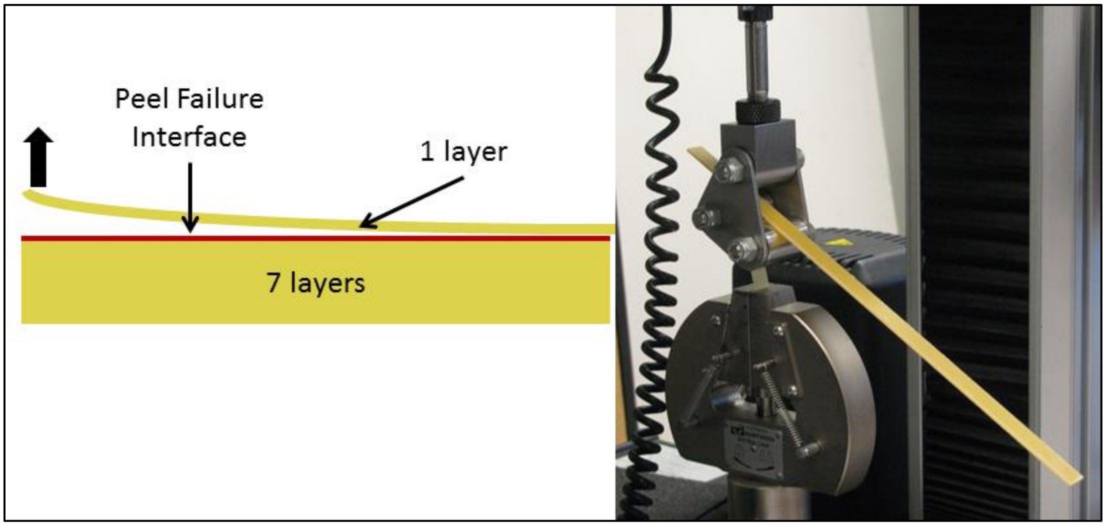

Figure 4.7: Floating Roller Peel Specimen and Setup

Once tested, the failure surfaces of each sample were imaged. At least two representative samples from each set were photographed from a location mid-way in the peel. For imaging, a Keyence™ VK-X200 series microscope was used with a 10X optical lens. Both surfaces were imaged with the bottom 7 layer portion of the peel sample still containing the tested material. Figure 4.8 shows example photos of the bottom peel surfaces taken with a camera. Further discussion of failure from imaging is located in Chapter 5.1.1.

Figure 4.8: Example Floating Roller Peel Failure Surfaces Taken with Camera

4.3.1.2 Short Beam Shear Sample Fabrication and Testing Description

Short beam shear was done to compare the shear strength and failures of our materials within the midplane of a composite laminate stack according to ASTM D2344. [34] Composite stacks were made to be 24 layers thick yielding a 0.64 cm (1/4 inch) thick composite. Every eight layers were debulked as mentioned earlier, before being placed together. The layer or material to be tested was placed within the midplane of the stack. Following the ASTM standard, the samples were cut to be six times the thickness in length and twice the thickness in width. A diamond saw slot grinder was used to cut these samples with automated feed cutting 0.025 cm every other pass to ensure surface smoothness. Samples were tested using a 5567 Instron™ and the span of the lower point contacts set to four times the sample thickness. A layer of thick Kevlar followed by rubber was used on the upper contact to reduce premature failure due to crushing locally. This cradled a 1.27 cm (0.5 inch) diameter steel pin versus the 0.64 cm (0.25 inch) pin recommended in the standard. This setup was found after a few trial tests to reduce local crushing failure best, forcing samples to fail in shear.

Figure 4.9 shows a schematic and the actual test setup of the SBS test including the larger top pin.

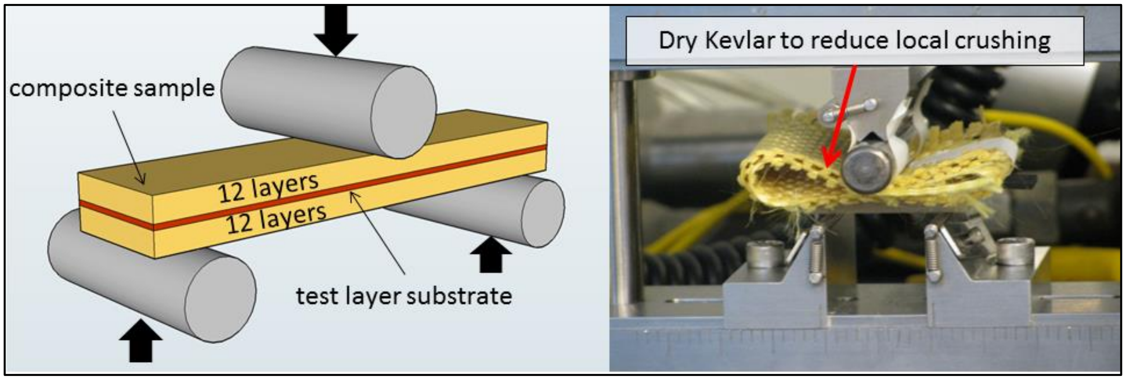

Figure 4.9: Short Beam Shear Testing Setup

Once tested, samples were then photographed with a camera. Failure crack location and orientation in the sample were noted. The sides of the samples were dyed to give better contrast between failed and unfailed regions. For this a blue dye was diluted with water and applied using a cotton swab. Once the dye soaked into the cracks it was then cleaned off of the surface with a damp paper towel. From here the failure location could be seen and compared between sample materials.

4.3.2 Mechanical Property Testing and Measurement

Once the interlaminar failure modes were determined, mechanical properties were measured which then can be used to predict the response of the completed sandwich structure. Tension testing followed the ASTM D3039 standard [35]. Tension samples featured a 2.54 cm (1 inch) sample gage width adequate to fit a representative area of FSS patches. Compression values were measured using ASTM D3410 [36]. This property is most susceptible to loss due to the inclusion of the FSS film. Failure in compression often occurs due to buckling. This is greatly affected by the interlaminar bond of the composite and the location where the FSS was placed.

A 2.54 cm (1 inch) square gage length was chosen for the compression test, to maximize available area for FSS patches. For both tension and compression testing, the substrate tested was placed within the midplane to keep loads symmetric although there is motivation for asymmetrical placement in electromagnetic design.

Chapter 5

LAMINATE MECHANICAL TESTING RESULTS

Testing began with ultrasonic C-scanning to look for large voids and inconsistencies. This was followed by burn-off of random samples within each panel to measure Fiber Volume Fraction. Below, in Table 5.1, are each of the mechanical tests with average dimensions, substrate location, and number of test scenarios. Results of mechanical testing reported with one standard deviation.

Table 5.1: Fabricated Composite Panel Specifications Used in Testing

Name	**Number of Layers**	**Average Thickness (cm)**	**Average FVF (%)**	**Substrate Location**	**Number of Scenarios**
Floating Roller Peel	8 layers	0.21 cm	44.2 %	Between 7th and 8th layer	9
Short Beam Shear	24 layers	0.67 cm	44.3 %	Midplane	9
Tension	8 layers *2 layers*	0.22 cm *0.06 cm*	46.7 % *51.4%*	Midplane	4
Compression	16 layers	0.44 cm	46.3%	Midplane	8

5.1 Adhesion Comparison of Baseline Composite and Printed Circuit Board Substrate Variants

Adhesion testing is a direct means of looking at how the embedded substrate interacts with the surrounding composite and was compared to the baseline composite without embedded material. From here the proposed substrate, on which to etch the FSS designs, can be thoroughly compared through every step in PCB processing. This proceeds from constituent materials used in the Pyralux™ to treatments used in improving bond strength, all the way through etching, and the final FSS layer.

5.1.1 Peel Strength Comparison

Average peel strength was measured for the baseline composite and then compared to the samples with added films and materials. First, the copper foils and Kapton films were compared with peel strength, results in Table 5.2 and Figure 5.1. The copper foils were made by Oak-Mitsui featuring untreated copper and the treated copper DBT-III. As mentioned earlier, the DBT-III features a surface treatment on the outside and inside of the roll. Untreated copper as well as the treated copper foils had bond strength just as high as the baseline. Although the drum side is smooth, it does have a slight roughness which can be attributed to higher bond strength. The datasheet reports a surface roughness value (Ra) of 0.245 microns (10 μ inch) while the treated side is 0.762 micron (30 μ inch). For this composite system and processing, this surface roughness was sufficient to give good peel strength. The plain Kapton film did not bond very well failing at nearly ¼ the baseline strength. However the corona plasma treated Kapton FPC bond strength was nearly that of the baseline. The failure of crack opening appears to happen easily along the untreated Kapton bond to the composite. Higher surface energy of the Kapton, due to the corona treatment improves this bond and increases the energy needed break it. This emphasizes the need for chemical treatment to improve peel strength of the Kapton films.

Table 5.2: Baseline Substrate Average Peel Strength

	Material	Strength (N/cm)
	Baseline Composite	20.7 ±1.1
Copper Substrate	Untreated Drum Side Copper	21.2 ±1.3
	DBT-III Outer	20.6 ±1.0
	DBT_III Inner	24.1 ±1.1
Kapton Substrate	Kapton	6.3 ±0.4
	Kapton FPC	19.4 ±1.7

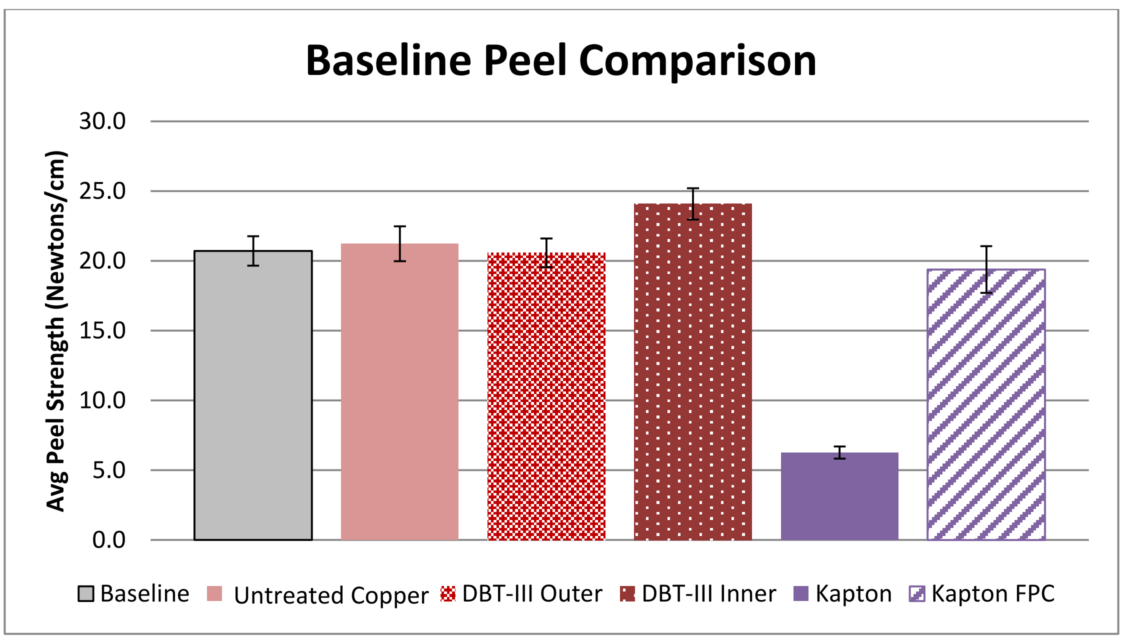

Figure 5.1: Baseline Material Peel Strength

Next the copper-clad system of Pyralux LF was tested in peel, with the results in Table 5.3. This film features both treated copper and Kapton film which from the baseline tests proved well for bonding. First the film was tested as received and the bond strength was slightly less but similar to the composite baseline. Since the etching procedure used to make the FSS exposes the film to a chemical bath, another set of peel samples were made. These samples of the Pyralux® film that had been exposed to the etchant solution much like the final FSS except the copper side was not etched. Average bond strength was the same as the baseline and slightly higher than the fresh Pyralux® film. Knowing that the etching solution will not adversely affect peel strength, we tested one of the FSS cases. This case had 4mm patches spaced 9.06 mm apart which corresponds to a 22.3% copper patch area on the fail surface. The peel strength was just as high as the baseline although with a slight increase in standard deviation.

Table 5.3: Pyralux™ Average Peel Strength ± One Standard Deviation

	Material	**Strength (N/cm)**
	Baseline Composite	20.7 ±1.1
Pyralux™	Kapton Side	17.9 ±1.1
	Copper Side	18.8 ±1.0
	Kapton Side After Etch	20.5 ±1.2
	Copper Side After Etch	21.4 ±1.1
	FSS 4mm-9.0mm	23.1 ±2.0

Failure surfaces were imaged and the bond interfaces noted. Failure regimes can be split into two categories; adhesive failure and cohesive failure. Adhesive failure occurs within the bond between two different materials. Cohesive failure occurs within two similar materials such as resin to resin. The baseline composite failed cohesively within the interlaminar resin region.

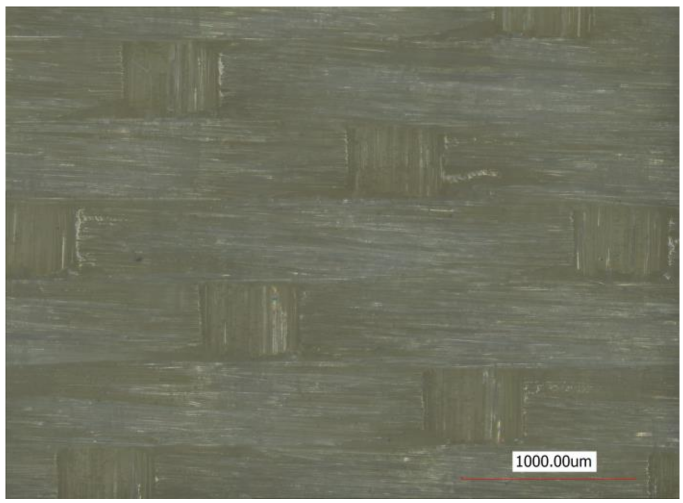

Figure 5.2: Baseline Floating Roller Peel Failure Surface

Figure 5.2 shows an image of the baseline failure surface. The copper foils failed similarly to the baseline, leaving resin residue on both surfaces. The untreated copper surface bonded well, failing mainly in the resin-to-resin region, which can be seen as the darker patches on the left image in Figure 5.3 with adhesive failure showing up as a lighter color. Surface roughness proved high enough such that the surrounding resin was able to bond to the copper surface. The amount of cohesive failure was enough to give this untreated drum side copper peel strength comparable to the baseline. The treated copper foil surfaces featured a very high surface area and gave very good mechanical bonding to the cyanate ester resin system. The right image in Figure 5.3 shows the peel fail surface of the treated copper drum side. This was much like the failure region for the baseline composite showing no adhesive failure between the resin and the copper.

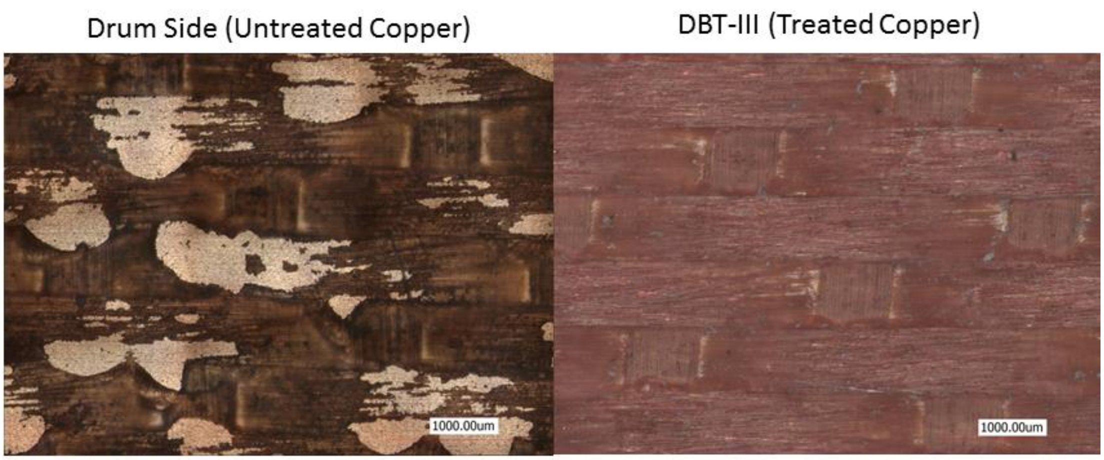

Figure 5.3: Copper Peel Failure Surface Comparison

In the case of the Kapton, films chemical treatments are needed to improve surface energy for adhesives. The untreated Kapton showed extremely poor bonding and failing adhesively between the resin and film surface. This was compared to Kapton FPC which was chemically treated and bond strength reached nearly that of the baseline yet still not as good as copper. Failure region was similar as the copper failing cohesively within the resin region although a few areas of exposed Kapton can be seen. All cohesive failures left resin on the actual test material as seen from the peel surface Figure 5.4.

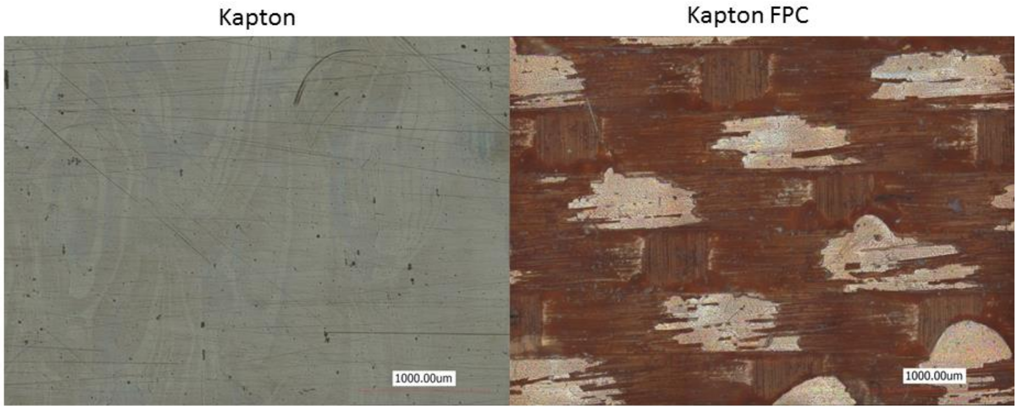

Figure 5.4: Kapton Peel Failure Surface Comparison

Bonding of the FSS case was also comparable to what was seen in the baseline composite. Failure was primarily cohesive in the resin region much like the other materials with good bond strength although some debonding was seen on the patches. In Figure 5.5 there were areas of exposed copper similar to the bond surfaces of the rolled copper. This difference in bond failure happened due to the etching procedure changing the surface characteristics of the electrodeposited copper on the Pyralux®.

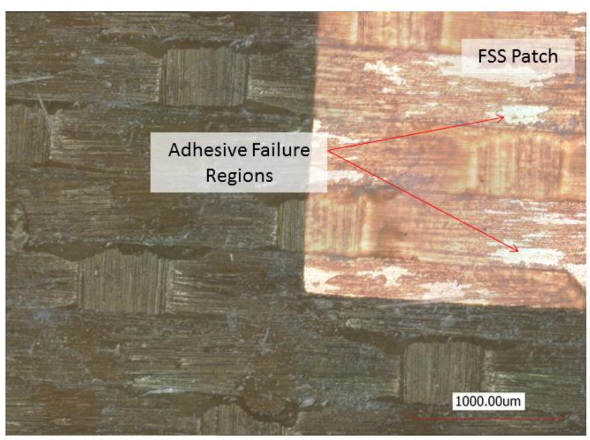

Figure 5.5: FSS Floating Roller Peel Failure Surface

5.1.2 Short Beam Shear Strength Comparison

Short beam shear test was used to compare the mode II shear strength in the materials studied. The same materials as used in the peel testing were tested here. Starting with the pure composite baseline we moved on to copper and Kapton followed by their surface treated derivatives and finally to one case of the FSS. Their relative strengths can be seen explicitly in Table 5.4 and graphically in Figure 5.6. There was a large decrease in strength for the untreated copper which earlier proved moderately well in peel bonding. The Kapton, which performed badly in peel, did much better in shear.

Table 5.4: Short Beam Shear Baseline Substrate Average Strength and ± One Standard Deviation

	Material	**Strength (MPa)**
	Baseline	12.1 ±0.2
Copper	Untreated Drum Side Copper	7.2 ±0.7
	DBT-III Outside	12.9 ±0.1
	DBT-II Inside	13.2 ±0.3
Kapton	Kapton	11.7 ±0.3
	Kapton FPC	12.2 ±0.3

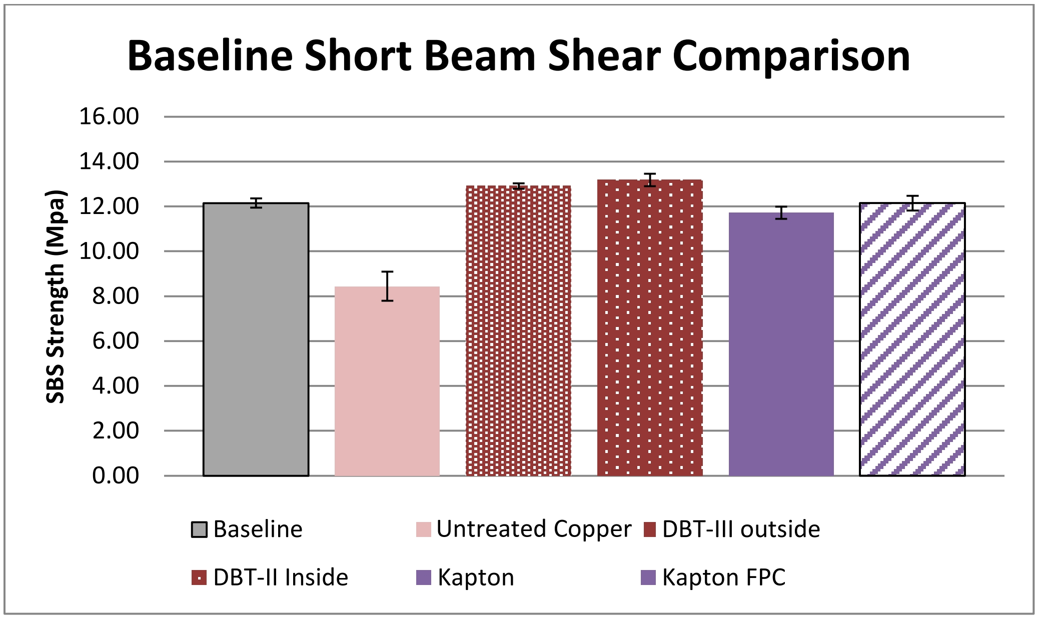

Figure 5.6: Short Beam Shear Strength Comparison

The Pyralux film, featuring both treated Kapton and copper, was tested by flipping the short beam shear samples to the other side. Short beam shear strength was very good and either met or exceeded the baseline strength seen in Table 5.5. The etched FSS sample's strength was very close to that of the baseline and confirmed that the etching process used on PCB materials as well as this FSS did not compromise short beam shear strength.

Table 5.5: Short Beam Shear Pyralux™ Substrate Strength and Standard Deviation

	Material	Strength (MPa)
	Baseline Composite	12.2 ±0.2
Pyralux™	Copper Side Up	12.6 ±0.2
	Kapton Side Up	13.0 ±0.2
	FSS 4mm – 9.06mm	12.6 ±0.3

Failure for these can be divided between bond failure at the mid-plane material interface and failure within the composite. Figure 5.7 lists materials, failure mode, and images of the failure. Blue dye was used to increase the contrast and make failure regions more apparent. Imaging was done macroscopically with a camera and further with a microscope. Microscope images focused mainly on comparing samples that had high short beam strength to the one that did not. Failure location is not easily apparent in Figure 5.7 for samples that failed in the midplane within the composite thus requiring further micrscopy. Samples were promptly removed from load once failure occurred. Under the same loading regime, the samples showed both failure within the midplane region as well as above and below the substrate. Samples that had high short beam shear strength showed failure that tracked away from the embedded substrate and into the surrounding composite.

Name	Failure	Photo
Baseline Composite	Composite	
Untreated Copper	Bonding	
Kapton	Composite	
Treated Copper	Composite Above and Below	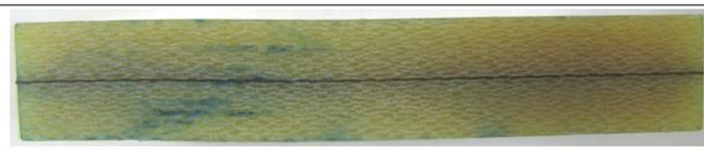
Treated Kapton FPC	Composite	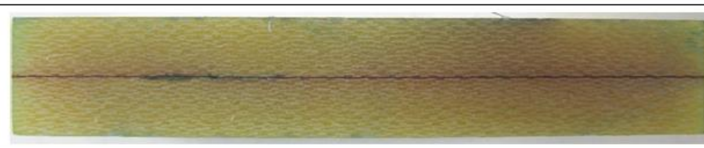

Figure 5.7: Short Beam Shear Baseline Failure Imaging

Failure locations for the Pyralux®-based materials can easily be seen. They occur within the actual composite which indicates they failed at strengths similar to the baseline. Figure 5.8 clearly shows the dyed cracks forming in the composite layers above and below the embedded film mid-plane. This failure tracking, from the measured strengths, can be attributed to good bond quality.

Name	Failure	Photo
Pyralux™ LF	Composite Above and Below	
Etched FSS 4mm-9.6mm	Composite Above and Below	

Figure 5.8: Short Beam Shear Failure Imaging Pyralux

Further failure damage was imaged using a microscope once the edges of the samples were polished. Blue ink was applied again to the samples to make cracks more apparent. The baseline sample failed within the midplane. A micrograph can be seen in Figure 5.9 with the crack tracking within the resin region between the fill direction tows of fiber seen coming out of the page. This failure is indicative of good bond with the other substrate's short beam shear damage compared to that of the composite baseline.

Figure 5.9: Baseline Short Beam Shear Failure Micrograph 10X

In comparison, the short beam shear sample failures with the embedded substrates primarily showed failure within the composite except for the untreated copper, drum side. Untreated drum had lower strength compared to the composite baseline. A failure crack can be seen in the top image of Figure 5.10 extending along the interface between the composite and the copper foil. The bottom image shows the untreated Kapton case which had good short beam shear strength and the failure crack can be seen within the composite surrounding the substrate yet not along the bond of the substrate.

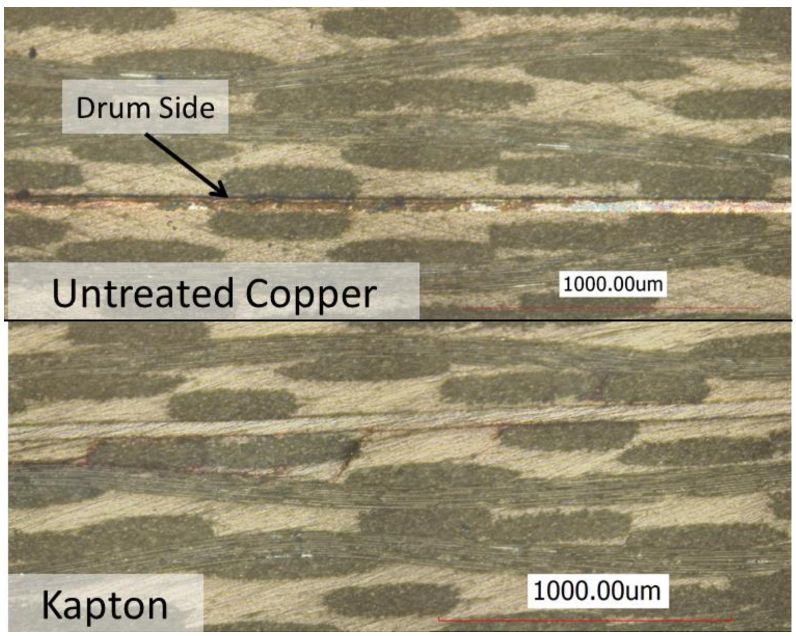

Figure 5.10: Untreated Copper and Kapton Short Beam Shear Micrographs 10X

All materials that showed good short beam strength failed within the composite region. Treated substrates, as well as the Pyralux™ system, failed in this manner within the midplane. The final FSS was no exception and can be seen Figure 5.11. Here the crack tracked within the composite, paralleling the embedded layer although not forming within the bond interface. The short beam shear failure regimes for the

Pyralux™ system as well as the surface treated substrates failed similarly to the baseline within the midplane. This emphasizes the need for surface treatments and confirms no loss in structural integrity when using these embedded systems.

Figure 5.11: FSS Short Beam Shear Micrograph 10X

5.2 Mechanical Property Testing and Comparison of Baseline Composite and Printed Circuit Board Substrate Variants

From adhesion testing one can move on to mechanical testing. The results of this can then be used for predicting the properties of a completed sandwich beam. The Pyralux™ showed good adhesive strength compared to the baseline composite and the next mechanical tests of tension and compression focus mainly on this system and the etched FSS layers.

5.2.1 Tensile Properties and Failure Discussion

Tension was less of a concern than compression due to the lack of failures attributed to debonding within the laminate but needed to be done to confirm the effect of the embedded FSS on tensile strength and stiffness. First the 8 layer case was tested comparing the baseline to the Pyralux® embedded in the composite mid-plane. As mentioned earlier, these samples often exhibited failure near the grips. This was also noted to happen through communication with Tencate® so a set of 2 layer samples were also tested. Table 5.6 shows the average strength and modulus of the tested samples with ± one standard deviation. The difference in mechanical properties versus the baselines was less than 7% with the inclusion of both the Pyralux™ and the Kapton. Thus adding the FSS layer within the composite laminate does not substantially deteriorate the mechanical properties.

Table 5.6: Average Tensile Properties of Baseline Composite and Pyralux™ System with Standard Deviation

Material	Strength (MPa)	Modulus (GPa)
Baseline 8 Layer	550.1 ±9.2	27.3 ±0.5
Pyralux™ 8 Layer	543.4 ±28.5	26.4 ±1.4
Baseline 2 Layer	597.2 ±22.4	29.8 ±1.6
FSS 3mm-6mm 2 Layer	555.5 ±16.0	28.8 ±1.9

Ultimate tensile strength for the 2 layer specimens was slightly higher than that of the 8 layer. There was a noticeable reduction in the thickness per lamina of the 2 layer meaning a higher fiber content which would result in a higher modulus and strength. Fiber volume content was measured via burn-off [31] to be 46.1% and 51.3% for the 8 layer and the 2 layer composite respectively. To better compare properties, the tensile strength and modulus was normalized by 50% fiber volume content using formula 5.1

.

$$x_{normalized} = x * \frac{FV_{common}}{FV_{actual}} \tag{5.1}$$

where:

x = Property to be normalized

FV_{common}= Common fiber volume fraction (50%)

FV_{actual} = Actual average fiber volume fraction measured

Table 5.7 shows the tensile strength normalized by the fiber volume content. The baselines and the Pyralux® strengths were very similar but a reduction could be seen for the FSS variant. For the same amount of composite material, the FSS did not reduce the strength greatly nor did the failure track the inclusion of the FSS.

Modulus faired similarly to the ultimate strength. The average modulus was still very near the range of one standard deviation of the baseline for the 8 layer and 2 layer samples respectively. The modulus normalized by fiber content, seen in Table 5.7, was very consistent showing nearly the same properties across the board. Altogether, the inclusion of the FSS layer did not greatly change the modulus of the composite.

Table 5.7: Tensile Properties Normalized by Fiber Volume Fraction

Material	**Normalized Strength (MPa)**	**Normalized Modulus (MPa)**
Baseline 8 Layer	588.9 ±6.5	58.5 ±1.0
Pyralux™ 8 Layer	585.5 ±30.7	58.2 ±3.1
Baseline 2 Layer	582.1 ±21.8	56.9 ±2.9
FSS 3mm-6mm 2 Layer	539.4 ±15.6	56.5 ±3.4

The failure damage in the tensile samples occurred independently of the inclusion of the FSS layer. Delamination of the embedded material did not occur as a result of failure. Failure occurred in the Pyralux and the FSS samples in the same manner as their baselines. In the end, none of the damage in the failure regions tracked the layer with the embedded FSS.

Most of the failures for these happened near the grips as seen in Figure 5.12. As for the 8 layer samples, failures near the grip were accompanied by some debonding of the outside layers of the composite. This can be seen in the bottom of the baseline samples #3 and #5.

Figure 5.12: Failed 8 Layer Tension Specimens

The two layer test was found to produce failures more consistently within the gage length versus the eight layer samples. The baseline, as well as one of the FSS scenarios, was tested this way as seen in Figure 5.13. For this case the FSS with 3mm patch size and a spacing of 6.8mm was chosen as it had the larger percent area of copper patches of 22.3%.

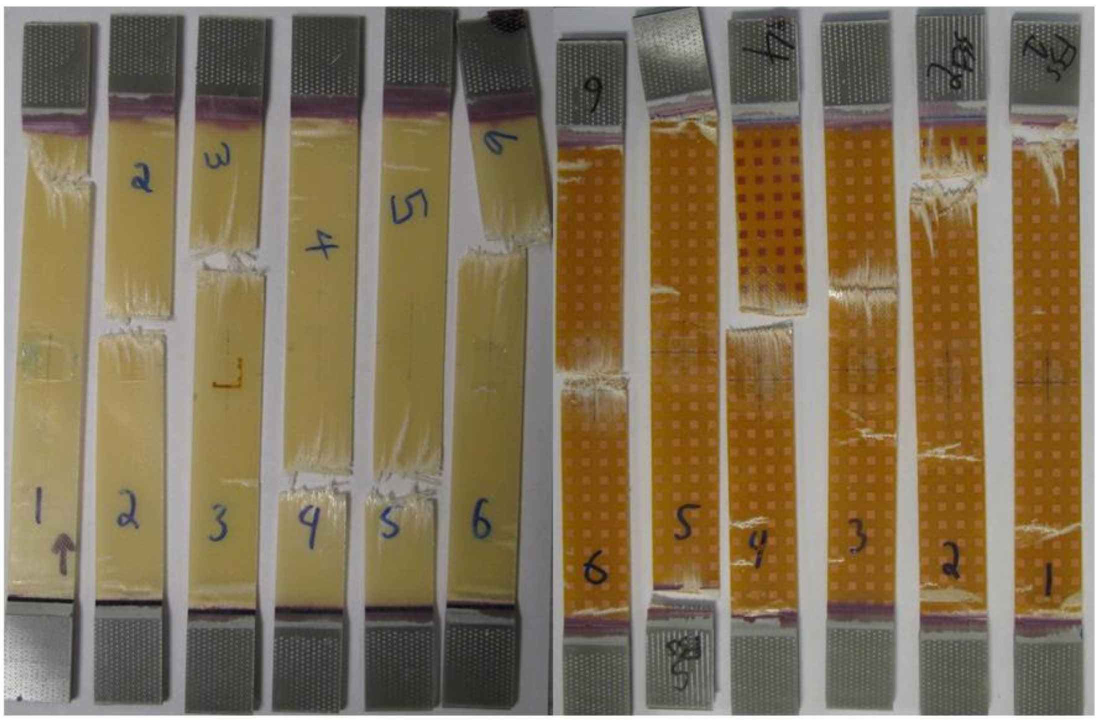

Figure 5.13: Failed 2 Layer Tension Specimens

5.2.2 Compressive Properties and Failure Discussion

Compression properties were measured in accordance with ASTM D 3410. All samples failed within the 2.54 cm (1 inch) gage length although many showed some bending (a percent difference between the strain gages). Reported values of strength and modulus come only from the samples that kept below 10% bending within the strain region outlined in the ASTM, 1000-3000 µstrain. Additional samples, other than the original 6, were made and tested for batches that exhibited bending. Fiber volume content was consistent for these samples and found to be 46.4% through burn-off measurements. Table 5.8 contains the average strengths and moduli as well as the percent difference compared to the baseline composite ± one standard deviation. Both properties were no more than 9% of the baseline composite.

Table 5.8: Average Compressive Properties and Standard Deviation

Material	**Strength (MPa)**	**Modulus (MPa)**
Baseline	553.8 ±31.3	26.4 ±2.2
Kapton	567.1 ±10.0	27.3 ±0.4
Pyralux®	565.1 ±16.4	27.9 ±0.3
FSS 3mm-6mm	567.9 ±7.5	26.5 ±0.3
FSS 4mm-9mm	540.2 ±26.3	27.3 ±0.9
FSS 3mm-9mm	577.3 ±25.1	28.3 ±0.8
FSS 2mm-9mm	554.9 ±20.0	27.5 ±0.6
FSS 3mm-13mm	599.0 ±27.0	28.7 ±0.9

Compressive strength of the FSS samples were compared to that of the baseline composite, Kapton, and the Pyralux™ cases. Figure 5.14 compares the strength values as well as standard deviation. Here the three baseline materials are shown first, followed by the FSS's in order of decreasing area percentage of patches. For the range of area percentages tested there was not a large decrease in strength versus the baseline. The FSS samples exhibited a slightly higher standard deviation with a decrease in copper. With a reduction in copper there was an increase in the surface of the Kapton that was etched off which may cause a higher variation in bond strength. This increase in standard deviation could also be seen in the FSS peel test.

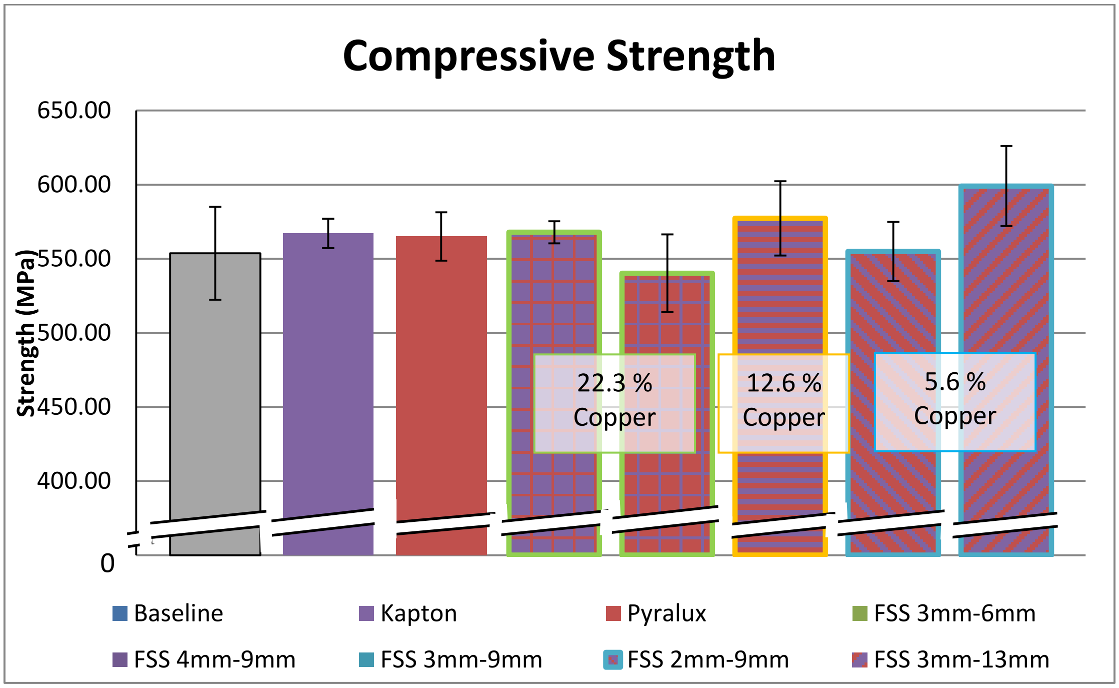

Figure 5.14: Compressive Strength

Modulus properties of the Kapton film, Pyralux™, and the FSS's were similar to that of the baseline as seen on Figure 5.15. The inclusion of a material within the midplane does not affect modulus. The average properties were still within the standard deviation of the baseline and there was very little trend based on the area percentage of copper patches in the FSS.

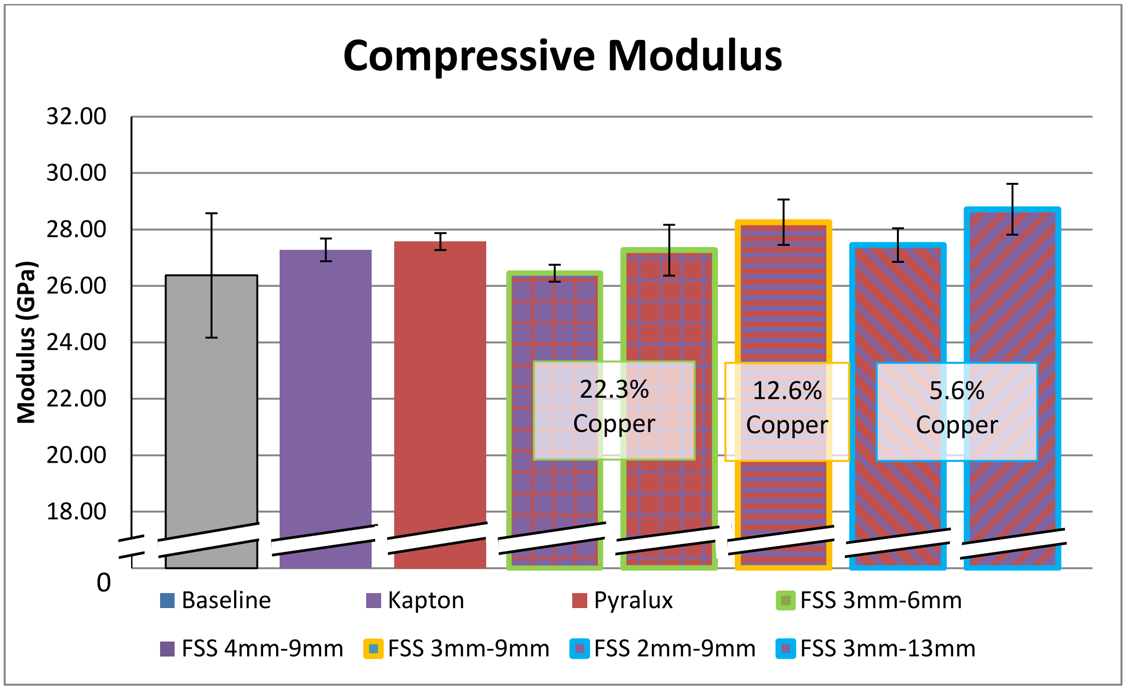

Figure 5.15: Compressive Modulus

The failure of each case of specimen was imaged. All samples failed properly within the 2.54 cm (1 inch) gage length with few or no failures close to the end tabbed regions. Focus was on the failure within the lamina which was best viewed right after failure before releasing the load on the sample.

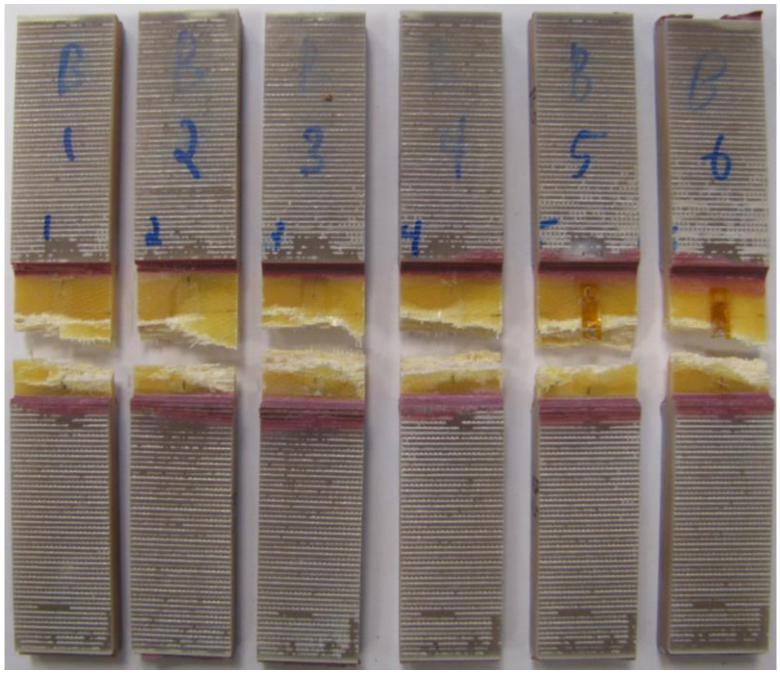

Figure 5.16: Failed Baseline Compression Samples

First the baseline composite was tested, shown in Figure 5.16, and compared to the untreated Kapton™ film. They both failed at similar strengths but the Kapton samples showed delamination within the Kapton film interlayer upon failure. This can be seen in Figure 5.17 where the Kapton case in the middle shows a large delamination in the film to composite bond region while the baseline showed debonding in the composite regions away from the midplane. While the location of the film in the midplane minimizes this effect, asymmetric designs may show reductions in properties due to premature delaminations. Next, the Pyralux™ film was tested. Once again, for the materials that bonded well in previous tests, most delaminations due to failure occurred within the composite versus the materials with poor bonding where delaminations were most likely to occur along the bond region.

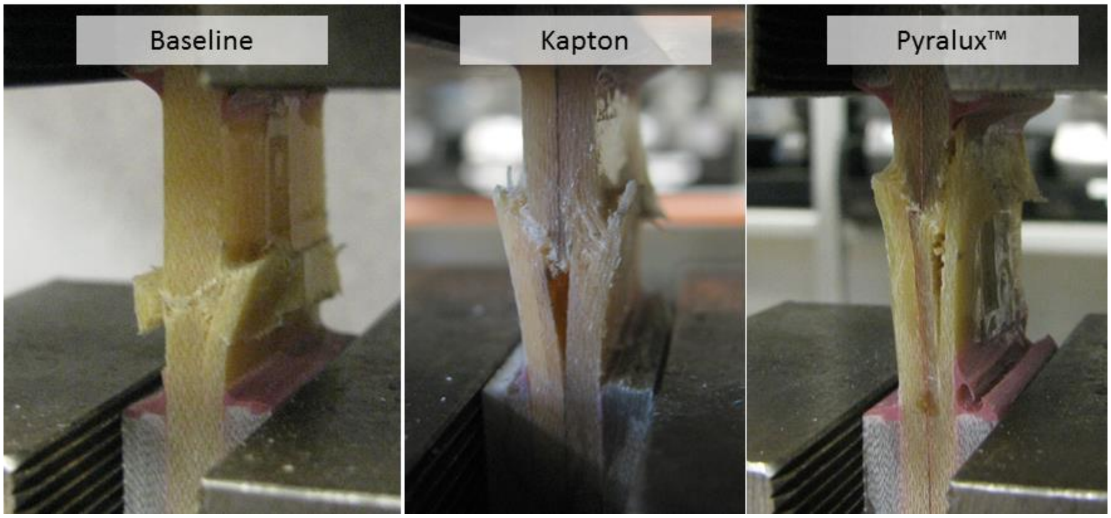

Figure 5.17: Compression Baseline Failure Comparison

Next the FSS compression samples were tested featuring the etched Pyralux™. Failure damage can be seen in Figure 5.18 where the images are in order of decreasing copper patch area percentage. The failure regions were similar to the Baseline and the Pyralux™ samples. Damage from delamination in failure occurred within the composite region for all of the FSS samples.

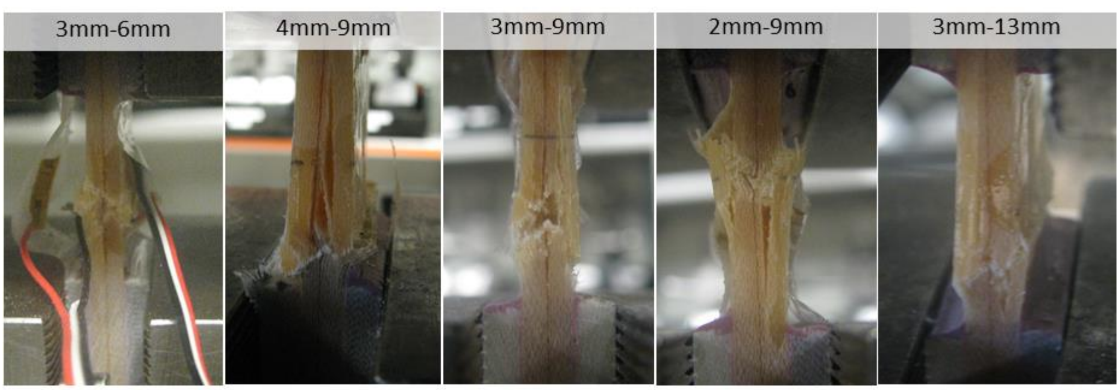

Figure 5.18: Compression FSS Failure Comparison (in order of decreasing patch area)

Chapter 6

SANDWICH DESIGN AND TESTING FEATUREING AN EMBEDDED FREQUENCY SELECTIVE SURFACE LAYER

Once the mechanical properties were measured, a complete sandwich structure was designed. This design features the FSS layer within the composite face sheets of the sandwich. Design focused on failing the sandwich in the face sheet to compare a baseline composite versus one of the FSS scenarios. Testing of this structure followed ASTM C393 using a three point bend [37] . Mechanical properties, such as bending stiffness and strength were predicted and then compared to the actual measured values.

6.1 Materials and Processing for a Sandwich Panel with Frequency Selective Layer

The mechanical properties of a composite sandwich beam can be predicted using the properties of the constituents. These include the mechanical properties of the face sheets and the core as well as the area moment inertia of the sandwich's cross-section. The face sheet properties are well known from the testing in the previous chapter. It is this location where the FSS layer is placed and the comparison made versus the purely composite baseline.

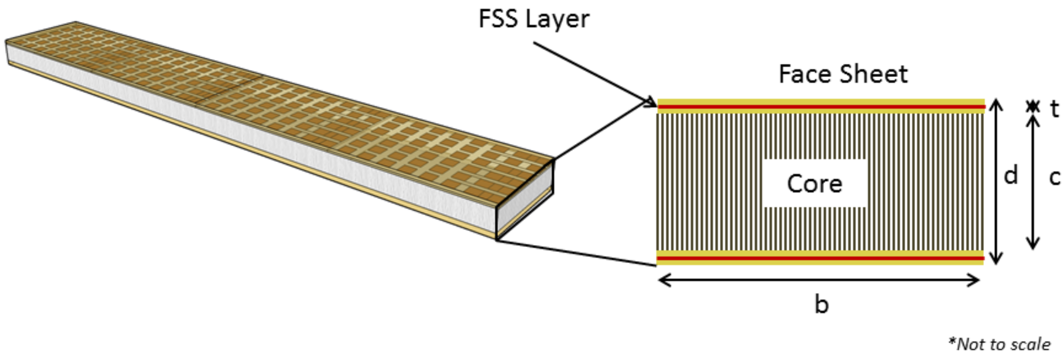

Figure 6.1: Sandwich Structure and Cross-Section Geometry

From beam theory, bending stiffness as well as the failure load of the beam can be predicted. Dimensions used in these calculations can be seen labeled in Figure 6.1. It is assumed that the face sheets carry the entire load. This is a common assumption made for sandwich beams with the criteria that the core to face sheet thickness ratio is greater than 5.35 [1] [10]. The area moment of inertia can be coupled with parallel axis theorem to calculate the area moment of inertia in Equation 6.1.

$$I = \frac{bt^3}{6} + \frac{tbc^2}{2} \tag{6.1}$$

where:

I = area moment of inertia

b = sandwich width

t = face sheet thickness

c = core thickness

From here the bending stiffness (EI) can be calculated. This is useful in comparing the stiffness response of the composite sandwich within the linear elastic regime. It is in this regime that the sandwich structure is loaded during actual service. Bending stiffness can be calculated by knowing the load and displacement of the beam in testing in Equation 6.2.

$$EI = \frac{PL^2}{48w} \tag{6.2}$$

where:

EI = bending stiffness

P = load

L= span

w = displacement at mid-span

Failure loads can also be predicted using beam theory. ASTM standard C393 for flexural testing of sandwich beams provides expressions for beam theory focusing on face sheet and core stresses [37]. As mentioned earlier, the top and bottom face sheets are assumed to carry the bending load in compression and tension respectively. The stress in the face sheets can be found in Equation 6.3. Knowing the ultimate stress of the composite face sheets, one can solve for the failure load P.

$$\sigma = \frac{PL}{2t(d + c)b} \tag{6.3}$$

where:

σ = stress

P = load

d = sandwich thickness

I = area moment of inertia of the beam

The core functions to spread the load from face sheet to facesheet via shear. Core failure load was predicted using the equation provided in the ASTM standard for core shear stress, Equation 6.4.

$$\tau = \frac{P}{(d + c)b} \tag{6.4}$$

where:

τ = core shear stress

P = load

d = sandwich thickness

From these two expressions for face sheet and core stress, criteria can be made in beam design. To compare the effects of the added FSS layer, the face sheets must fail before the core. Knowing the failure stress, one can solve for the failure load for shear as well as tension and compression in the face sheets. Beam geometry can be iterated until predicted failure load of the core is much higher than the face sheet. This can be done by varying core thickness as well as beam span.

6.2 Core Material Selection and Sandwich Beam Fabrication

Materials chosen must also provide the necessary electromagnetic properties. This means the electromagnetic waves must be able to freely pass through the core as well as the composite with minimal loss. The two face sheets have the potential for placing two FSS layers within the sandwich structure. This is relevant in electromagnetic applications where multiple FSS layers can be used to filter out more than one frequency [5]. Here the FSS was placed within the midplane of each face sheet much like the previous tension and compression samples. Two layer face sheets were chosen because they could contain the FSS layer within the midplane as well as fail at a lower load then the chosen core material. The core must also be low loss, motivating the choice of a Nomex™ honeycomb core made by M.C. Gill Corp model HK-1/8-3.0.

Face sheets were made separately and then bonded to the core. These were made from the same prepreg system and following the same processing procedures as the previous test samples as stated in Section 4.1. Average fiber volume fraction for the face sheets was found to be 48.5% via burn-off, ASTM D2584. The surface of the face sheets were sanded using a 180 grit sand paper. Rymplecloth was then used to dry wipe the surface free of dust and debris. These sheets were then bonded to the core using Scotch-Weld™ AF563 film adhesive. The entire stack was placed under vacuum and cured at 121˚C (250˚F) for 120 minutes in an oven. Table 6.1 lists the materials used in the sandwich construction as well as thicknesses.

Table 6.1: Composite Sandwich Materials List and Thicknesses

	Material	Thickness	Notes
Facesheets	BTCy-1 Cyanate Ester S-glass	0.49 mm	FVF: 48.5%
Core	Gilcore HK-1/8-3.0	21.48 mm	
Film Adhesive	Scotch-Weld AF 563	0.432 mm	
Final Sandwich		23.24 mm	

The final sandwich panel was measured to be 2.31 cm thick. Sample width was chosen to be 5.08 cm (2 inches) to be at least twice the sandwich thickness. A span of 40.6 cm was chosen with 2.54 cm (1 inch) of beam overhang. This resulted in the overall sample length to be 45.72 cm (18 inches) long. This geometry reached the proper criteria to achieve face sheet failure before core failure. Samples were then cut using the diamond tipped wet saw cutting 0.025 mm each pass.

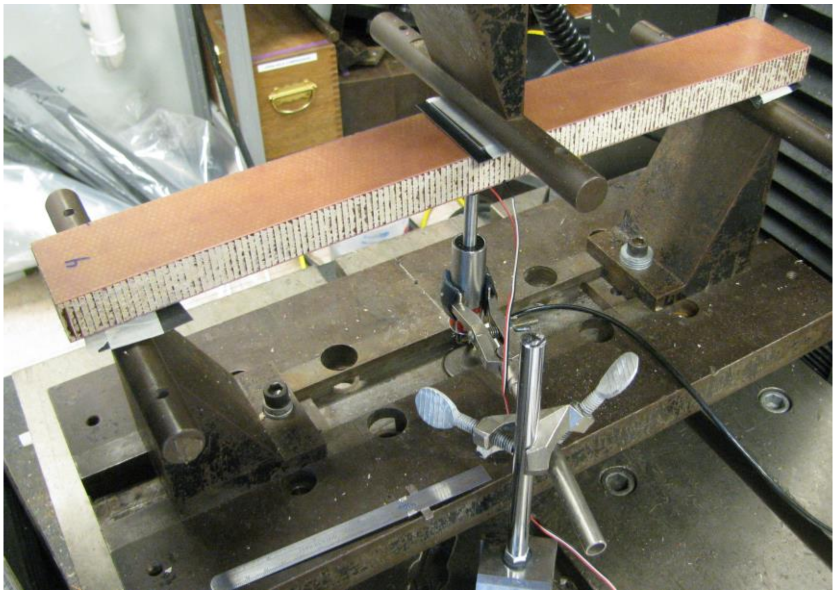

Figure 6.2: Three Point Bend Setup

Once the samples were let dry at room temperature, they were then measured and prepared for testing. Strain gages were placed on the bottom of each sample. For this, Vishay CEA-06-125UE-350 gages were used and aligned in the direction of the sample span. An LVDT was added and contacted a point next to the strain gage. The LVDT was made by RDP Group model DCTH300AG. This was used to measure the extension and removed before ultimate failure of the sample. The entire setup can be seen in Figure 6.2 with wires going to the bottom strain gage and the fixed LVDT in contact with the bottom of the sample. The FSS patches were aligned so that the line of patches was symmetric with the loading point and support span.

Samples were tested in three point bend at a crosshead rate of 1.27 cm/min (0.5 inch/min). The contact supports were 1.27 cm (0.5 in) diameter steel cylinders. These were found to cause premature failure in the core due to load concentration so 2.54 cm (1 inch) wide steel pads were used with a rubber pad contacting the sample. The latter configuration was found to fail samples consistently in the face sheets without any premature failure in the core. A total of three samples were made of the baseline and the FSS scenario. The number of samples was limited to three due to limitations in the FSS layer size.

6.3 Testing and Results

Both the baseline and the FSS sandwiches failed within the face sheets. 6.2 shows the bending stiffness and failure load of the composite sandwich samples as well as the predicted values within one standard deviation. Bending stiffness followed theory well resulting in a percent difference no greater than 7%. The beam bending failure loads, as well as the face sheet stresses at failure, were lower than the predicted. Predicted values were calculated from failure stresses of the before mentioned compression tests. Yet the failure loads and stresses of the baseline and the FSS sandwich are very similar proving that the inclusion of the FSS layer did not detrimentally affect failure load versus the baseline.

Table 6.2: Three Point Bending Stiffness and Failure Loads

Scenario	**Bending Stiffness ($N * m^2$)**	**Failure Load (N)**	**Face Sheet Failure Stress (MPa)**
Predicted	*168.5*	*3045.3*	*553.0*
Baseline	176.9 ±2.0	2214.9 ±65.7	396.5 ±11.2
FSS	179.2 ±1.6	2284.6 ±11.1	416.0 ±2.7

Deflection of the beam was measured using the Instron crosshead displacement as well as LVDT. These two values correlated well so crosshead displacement was used in comparing the baseline against the FSS sandwich beam. Load and crosshead extension from representative samples was compared between the two within the linear elastic region in Figure 6.3. The beam with the embedded FSS layer responded nearly identically to the baseline composite.

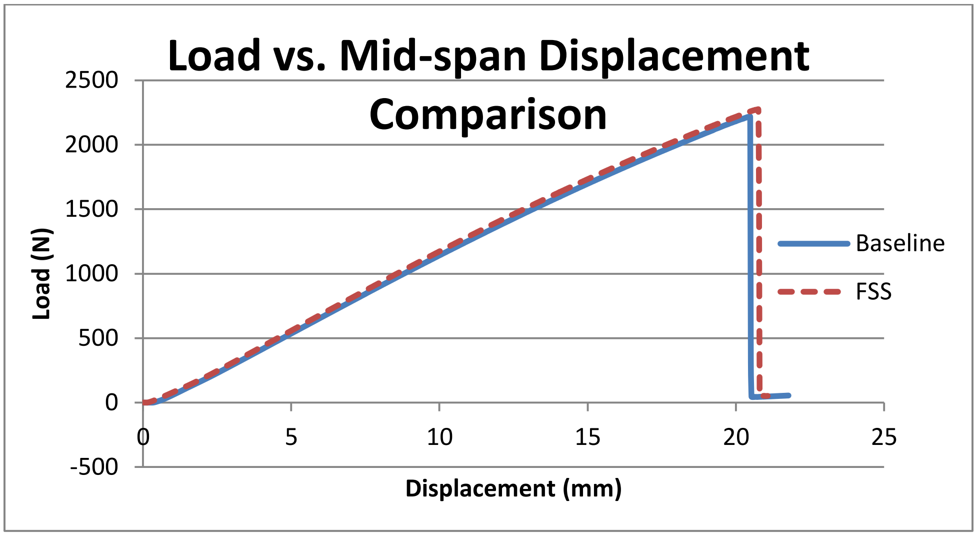

Figure 6.3: Load vs. Extension Response of Sandwich Beams

Failure occurred at a lower load than the theory predicts. The failure location was closer to the ends of the steel pads than it was to the actual center of the beam. This prematurely concentrated the stress there and failed the beams. Figure 6.4 shows the failure locations. Damage appears similar between the Baseline and the FSS. Delamination did occur during failure but both shared the same extent of damage. Representative side images of the sandwich failures can be seen in Figure 6.5 for both the baseline and the FSS sandwich beam. Face sheet failure is obvious with little distortion in the core.

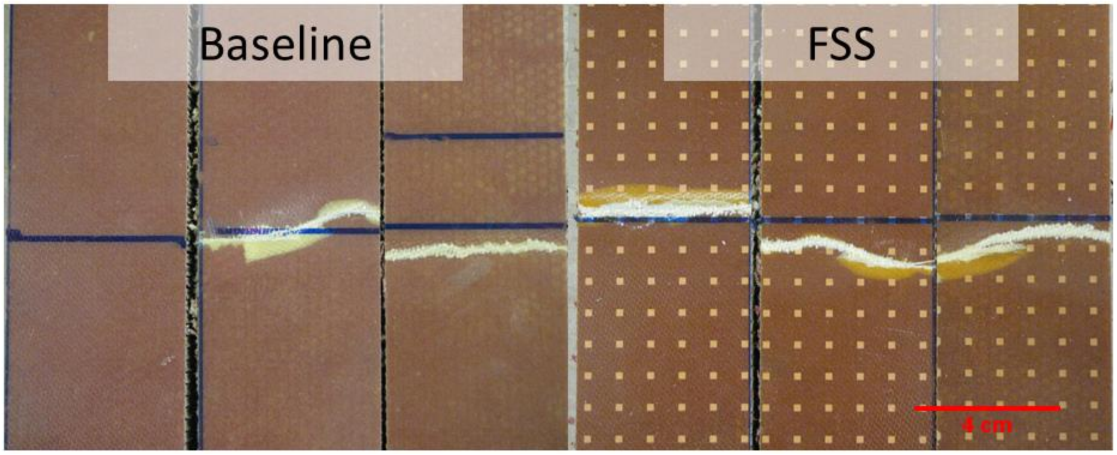

Figure 6.4: Three Point Bend Failure Images

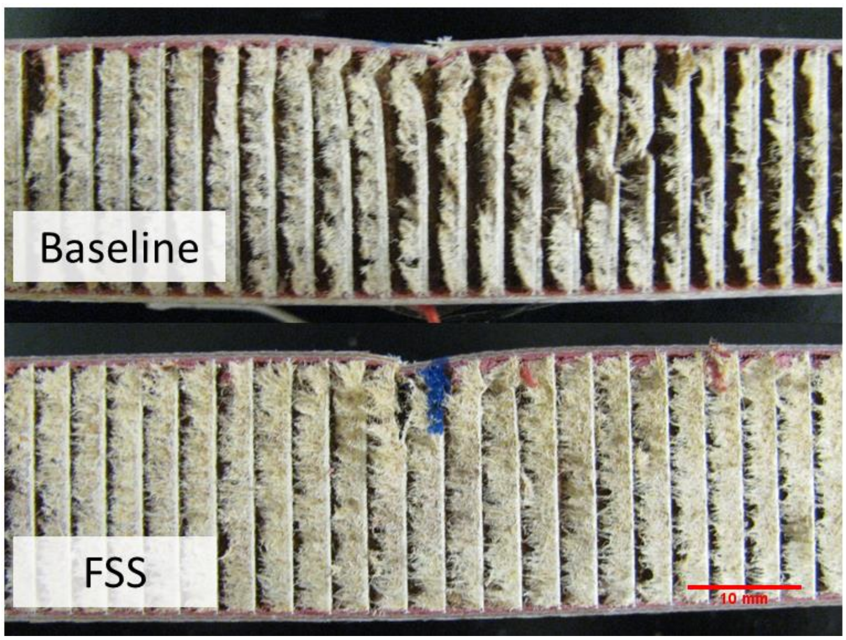

Figure 6.5: Sandwich Specimen Failure Viewed from Side

Chapter 7

CONCLUSION AND FUTURE WORK

7.1 Conclusion

For this specific multifunctional material with FSS geometry there was no measurable loss in mechanical properties compared to the baseline structure without embedded substrates, within statistical bounds. The FSS materials chosen were commonly used in PCB fabrication and had been proven to perform well for adhesion in the composite system. Emphasis was placed on surface treatments of the FSS materials; in this case Kapton film and the copper foil. Preliminary tests on these materials showed how important surface treatments are to bonding in both peel and shear modes. The mechanical properties measured in tension and compression did not change compared to the baseline. The Kapton compression samples did show a large delamination between the composite region and the embedded Kapton film shortly after failure. However this did not affect the mechanical properties. In the case of sandwich structures, given this specific FSS design and substrate, this works shows that one can design in the same manner that one would have used if there were no embedded FSS layer.

Presented here is a testing methodology starting with bond strength and failure mechanisms before proceeding to mechanical properties used in the design of composite sandwich structures. This methodology was applied to design of a sandwich featuring an embedded FSS layer. For the inclusion of a new material within a composite laminate, bond strength is a big concern. The proposed methodology in this work focuses on comparing adhesion failure characteristics to validate and improve material selection before mechanical tests are done. Tests can be done, such as peel and short beam shear, to compare the bond strengths of various materials. After that work, one can more easily determine which materials should be used in the final tests of tension and compression to ultimately predict the composite sandwich structure's mechanical response.

7.2 Future Work

There are many ways to expand on this research. Here the focus was on one variety of electromagnetically functionalized material for use in a specific application of sandwich structures for use in naval application. Further research could expand on different applications as well as other candidate materials. In this work, a standard PCB material performed comparably to the baseline composite. However, other material options exist possibly at lower cost and more scalable means of manufacturing.

7.2.1 Conductive Materials and Substrates

The conductive copper foils have very different mechanical properties than the surrounding composite. Loads encountered by the composite sandwich panel may be greater than the failure loads of the embedded copper causing delamination between the composite and the copper as well as ultimate failure of the copper. Previous research has been done for simple direct current conductivity along an embedded copper strip [23] but not for discrete patches. Here, cyclic loading testing of tensile and compressive regimes as well as the complete sandwich structure need to be done. Damage can be periodically measured using ultrasonic C-scans and in the anechoic chamber for changes in electromagnetic response. From these, internal adhesion failure can be observed as well as any degradation in EM response as a result of cyclic loading. Testing results shown in this work show good adhesion between the conductive FSS substrate and the surrounding composite. Cyclic testing would provide insight in adhesion strength to cyclic-induced bond failure as well as its role in any ductile failure in the copper which was observed in literature.

For these FSS layers a conductive substrate is needed. Copper etching is one method which can be done very well with high accuracy although there are other means of providing these conductive pathways. Conductive inks and powders can be used in the place of metal foils [38] [39]. These methods are additive versus the subtractive methods used in etching. They are still new to the science of electromagnetically functionalized materials as well as structural composites. The same extensive testing regime would be needed to confirm that they too do not adversely affect structural properties. Screen printing, shown in Figure 7.1, is one such way of applying conductive ink to either a film or fabric substrate. This method is common for making discrete patterns on textiles such as T-shirts although there are continuous ways to inking as well. Other benefits stem from processing as printing could be done through a roll-to-roll means of continuously applying the conductive pattern such as gravure printing. This would increase manufacturing efficiency versus etching discrete panels and laying them up piece by piece.

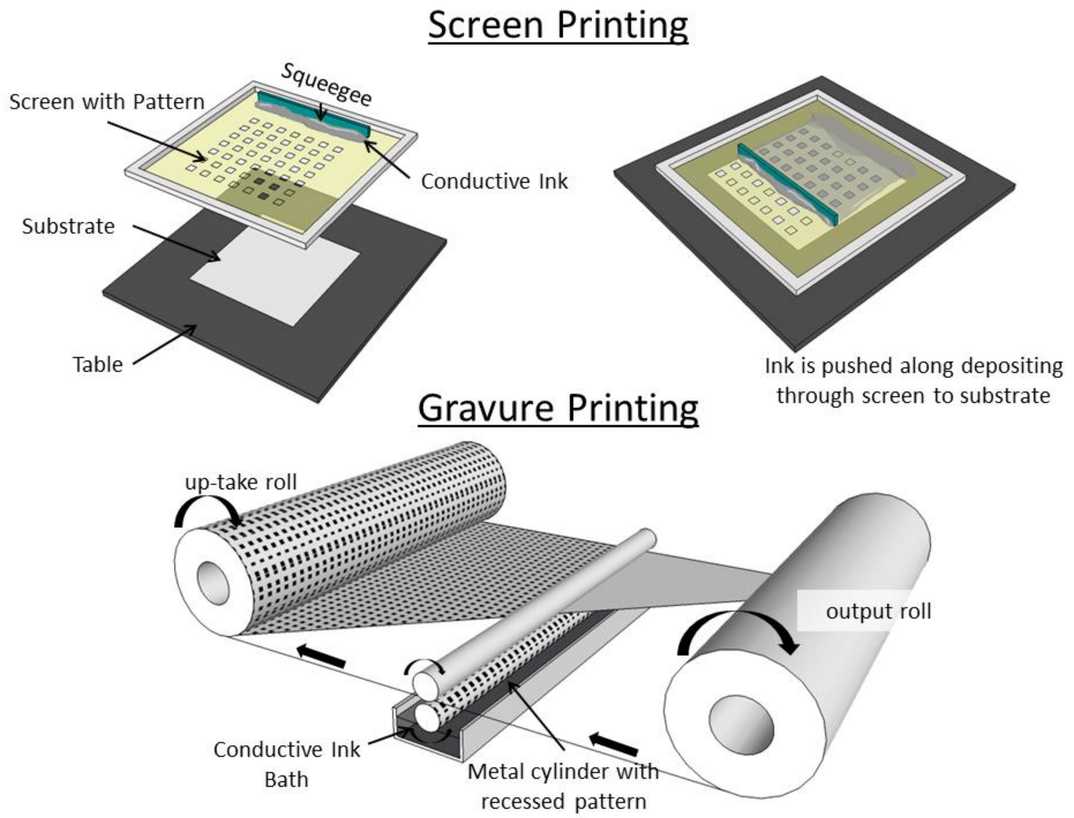

Figure 7.1: Methods of Conductive Ink Printing

Regardless of what conductive material is used, there must be a substrate to hold them in place. For the FSS design in this research a polymer Kapton film was used but there are other alternatives. An additive process, such as printing, could be coupled with other films, dry fiber, or even the prepreg itself.

7.2.2 Improvements in Testing

There are further mechanical tests that could be done for this specific application. The effect of the embedded FSS on shear could be studied with ±45˚ oriented tension samples. This means of off-axis loading is also relevant to sandwich structures though this study has only looked at the properties in the warp direction.

Mechanical testing done in this work has focused on symmetric substrate placement as well as loading. In the electrical regime, there are advantages to asymmetric electromagnetically functional layers. For the design of FSS materials, multiple layers can be combined in order to increase bandwidth filtering or to filter more than one discrete frequency [1] [5]. Figure 7.2 shows a cross section schematic of a composite with two FSS layers asymmetrically placed in reference to the centerline. Asymmetric interlaminar substrate placement may have detrimental effects to compressive strength where failure is susceptible to buckling failure. Thicker composite face sheets with multiple FSS layers placed asymmetrically would require additional testing in order to examine the effects this layup would have on the completed sandwich.

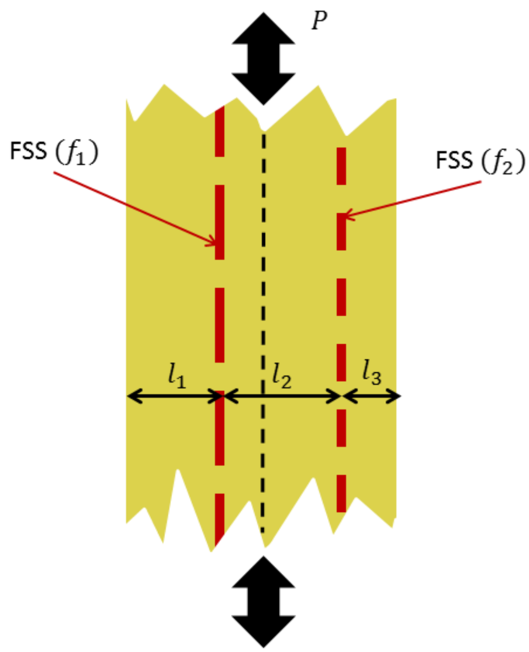

Figure 7.2: Composite Cross Section Schematic with Asymmetric FSS Placement Corresponding to Unique Resonant Frequencies

The emphasis of this research was on sandwich structures primarily for use in radomes. Other mechanical properties besides tension and compression may also be important. For example, panels made to withstand ballistic impacts would have an entirely different design criteria and set of tests to confirm the effects of an embedded electrometrically functionalized material.

7.2.3 Alternative Electromagnetic Structures

There are many structures used in making FSS materials. Solid square patches were just one geometry that were orthotropic and thus more conducive for testing mechanically. Other patch geometries could also be studied; for example tripoles and Jerusalem crosses, which perform very well as FSS's and takes up much less surface area then solid squares [5].

Other options include multilayer materials and asymmetric designs including through-thickness conductivity. Further 3D designs include High Impedance Surfaces (HIS) first studied by Sievenpiper [40]. An example of one of these can be seen in Figure 7.3. These surfaces have amplifying effects when coupled with an antenna and have traditionally been made from PCB materials. In the case of composite laminates, the conductive patches and ground planes can be coupled with through-thickness conductivity. This can be facilitated using drilled holes plated with copper or the structural composite analog of Z-pinning [41]. Drilled holes and through-thickness conductivity are common in PCB fabrication but have yet to be expanded to structural composites.

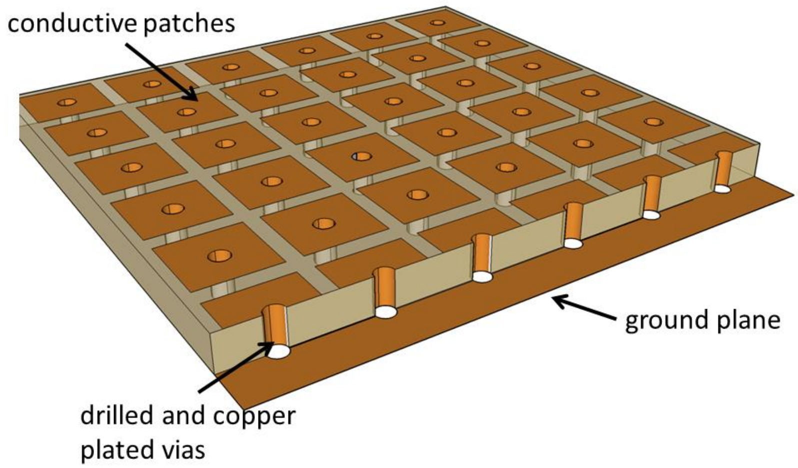

Figure 7.3: High Impedance Surface with Drilled Vias

REFERENCES

[1] L. Carlsson and G. Kardomateas, Structural and Failure Mechanics of Sandwich Composites, New York: Springer, 2011.

[2] J. R. Vinson, The Behavior of Sandwich Structures of Isotropic and Composite Materials, Lancaster, PA: Technomic Publishing Company, Inc., 1999.

[3] I. M. Daniel and J. L. Abot, "Fabrication, testing and analysis of composite sandwich beams," *Composites Science and Technology,* vol. 60, pp. 2455-2463, 2000.

[4] J. Tomblin, T. Lacy, B. Smith, S. Hooper, A. Vizzini and S. Lee, "Review of Damage Tolerance for Composite Sandwich Airframe Structures," U.S. Department of Transportation Federal Aviation Administration Office of Aviation Research, Washington, DC, 1999.

[5] B. A. Munk, Frequency Selective Surfaces Theory and Design, Danvers, MA: John Wiley & Sons Inc., 2000.

[6] R. Mittra, C. H. Chan and T. Cwik, "Techniques for Analyzing Frequency Selective Surfaces - A Review," *IEEE,* vol. 76, no. 12, 1988.

[7] R. Mittra, C. Tsao and W. Ko, "Frequency Selective Surfaces with Applications in Microwaves and Optics," in *IEEE MTT-S International*, Washington, DC, 1980.

[8] M. I. Montrose, Printed Circuit Board Design Techniques for EMC Compliance, Piscataway, NJ: IEEE Press, 1996.

[9] C. H. T. C. Raj Mittra, "Techniques for Analyzing Frequency Slective Surfaces - A Review," *Proceedings of the IEEE,* vol. 76, no. 12, pp. 1593-165, 1988.

[10] J. R. Vinson, Plate and Panel Structures of Isotropic, Composite, and Piezoelectric Materials, Including Sandwich Construction, Norwell MA: Springer, 2005.

[11] J. B. Birks, "Dielectric Housings for Centimetre-Wave Antennae Part: 2," *The Journal of the Institution of Electrical Engineers,* vol. 93, no. 4, pp. 653-657, 1946.

[12] P. A. Engel, Structural Analysis of Printed Circuit Board Systems, New York: Springer-Verlag New York Inc. , 1993.

[13] M. Lin and F.-K. Chang, "The manufacture of composite structures with a built-in network of piezoceramics," *Composites Science and Technology,* pp. 919-939, 2002.

[14] S. Nemat-Nasser, S. Nemat-Nasser, T. Plaisted, A. Starr and A. V. Amirkhizi, "Multifunctional Materials," *BIOMIMETICS: Biologically Inspired Technologies,* pp. 309-341, 2005.

[15] P. J. Callus, "Novel Concepts for Conformal Load-bearing Antenna Structure," DSTO, Fishermans Bend, Victoria 3207, 2008.

[16] A. Lockyer, K. H. Alt, D. Coughlin, M. D. Durham and J. N. Kudva, "Design and development of a conformal load-bearing smart-skin antenna: overview of the AFRL Smart Skin Structures Technology Demonstration," Northrop Grumman Corporation, Hawthorne, CA, 1999.

[17] K. Park, S. Lee and C. Kim, "Fabrication and electromagnetic characteristics of electromagnetic wave absorbing sandwich structures," *Composites Science and Technology,* vol. 66, no. 3-4, pp. 576-584, 2006.

[18] I. Choi, J. G. Kim, D. G. Lee and I. S. Seo, "Effects of a damaged composite face to the electromagnetic wave transmission characteristics of low-observable radomes," *Composite Structures,* 2011.

[19] T.-K. Wu, "Four-Band Frequency Selective Surface with Double-Square-Loop Patch Elements," *IEEE Transactions on Antennas and Propagation,* vol. 42, no. 12, pp. 1659-1663, 1994.

[20] P. C. Kim, D. G. Lee, I. S. Seo and G. H. Kim, "Nanocomposite stealth radomes with frequency selective surfaces," *Composite Structures,* pp. 299-305, 2008.

[21] W.-J. Lee, J.-W. Lee and C.-G. Kim, "Characteristics of an electromagnetic wave absorbing composite structure with a conductive polymer electromagnetic bandgap (EBG) in the X-band," *Composites Science and Technology,* vol. 68, pp. 2485-2489, 2008.

[22] A. A. Obaid and S. Yarlagadda, "Structural Performance of the glass fiber–vinyl ester composites with interlaminar copper inserts," *Composites Part A: Applied Science and Manufacturing*, vol. 39, no. 2, pp. 195-203, 2008.

[23] H. Kim, M. Park and K.Hsieh, "Fatigue Fracture of Embedded Copper Conductors in Multifunctional Composite Structures," *Composites Science and Technology,* vol. 66, no. 7-8, pp. 1010-1021, 2006.

[24] S. Lee, K. Oh and C. Kim, "Electromagnetic characteristics of frequency selective fabric composites," *Electronic Letters,* vol. 42, no. 8, pp. 12-14, 2006.

[25] Y. Zhou, Y. Bayram and S. Member, "Polymer-Carbon Nanotube Sheets for Conformal Load Bearing Antennas," *IEEE Transactions on Antennas and Propagation,* vol. 58, no. 7, pp. 2169-2175, 2010.

[26] Y. Zhou, Y. Bayram, F. Du, L. Dai and J. L. Volakis, "Polymer-Carbon Nanotube Sheets for Conformal Load Bearing Antennas," *IEE Transactions on Antennas and Propagation,* vol. 58, no. 7, pp. 2169-2175, 2010.

[27] L. Yao and Y. Qiu, "Design and Fabrication of Microstrip Antennas Integrated in Three Dimensional Orthogonal Woven Composites," *Composites Science and*

Technology, vol. 69, pp. 1004-1008, 2009.

[28] Tencate Advanced Composites Inc., "http://www.tencate.com," [Online]. Available: http://www.tencate.com/amer/Images/TCAC_Radomes%26AntennasGuide_Web_tcm29-23025.pdf. [Accessed 12 June 2013].

[29] K. Naito, Y. Kagawa and K. Kurihara, "Dielectric properties and noncontact damage detection of plain-woven fabric glass fiber reinforced epoxy matrix composites using millimeter wavelength microwave," *Composite Structures,* vol. 94, pp. 695-701, 2011.

[30] Tencate Advanced Composites Inc., "http://www.tencate.com," 3 2009. [Online]. Available: http://www.tencate.com/TenCate/Aerospace_composites/documents/TCAC%20USA%20docs/TCAC%20USA%20Datasheets/DataSheet/DS%20BTCY1%20Web.pdf. [Accessed 2012].

[31] ASTM D2584-02, *Standard Test Method for Ignition Loss of Cured Reinforced Resins,* West Conshocken, PA: ASTM International, 2002.

[32] ASTM D2734-94, *Standard Test Methods for Void Contest of Reinforced Plastics,* West Conschocken, PA: ASTM International, 2003.

[33] ASTM D3167-03a, *Standard Test Method for Floating Roller Peel Resistance of Adhesives,* West Conshocken, PA, 2004.

[34] ASTM D2344, *Standard Test Method for Short-Beam Strength of Polymer Matrix Composite Materials and Their Laminates,* West Conshocken, PA, 2006.

[35] ASTM D3039, *Standard Test Method for Tensile Properties of Polymer Matrix Composite Materials,* West Conshocken, PA, 2006.

[36] ASTM D3410D, *Standard Test Methods of Compressive Properties of Polymer Matrix Composite Materials with Unsupported Gage Section by Shear Loading,* West Conshocken, 2003.

[37] ASTM C393, *Standard Test Method for Flexural Properties of Sandwich Constructions,* West Conshohocken, PA: American Society for Testing and Materials International, 2000.

[38] M. Pudas, N. Halonen, P. Granat and J. Vahakangas, "Gravure printing of conductive particulate polymer inks on flexible substrates," *Progress in Organic Coatings,* vol. 54, no. 4, pp. 310-316, 2005.

[39] D. Sung, A. d. l. F. Vornbrock and V. Subramanian, "Scaling and Optimization of Graver-Printed Silver Nanoparticle Lines for Printed Electronics," *IEEE Transactions on Components and Packaging Technologies,* vol. 33, no. 1, pp. 105-114, 2010.

[40] D. Sievenpiper, *High-Impedence Electromagnetic Surfaces,* University of California Department of Electrical Engineering, 1999.

[41] R. McCauley, S. Yarlagadda, P. Pa, M. Mirotznik and M. Keefe, "Mechanical

Behavior of Composites Laminates with Electronic High Impedence Surfaces," in *Society for the Advancement of Materials and Process Engineering*, Newark DE, 2012.

Appendix A

RADIO FREQUENCY MATERIALS, MODELING, AND TESTING NOTES

Material selection stems from both the mechanical and the electrical regimes. In the case of the structural composite, traditional PCB materials can be used as a baseline, comparing the structural properties as well as the electromagnetic loss. Figure A.1 compares various PCB board materials versus the composite system studied in this research. The PCB boards are produced and measured by Rogers Corp.® and show very low loss as well as much lower strength compared to the cyanate ester/ S-glass composite system. This composite system was chosen for its high strength as well as low loss, comparable to the PCB materials.

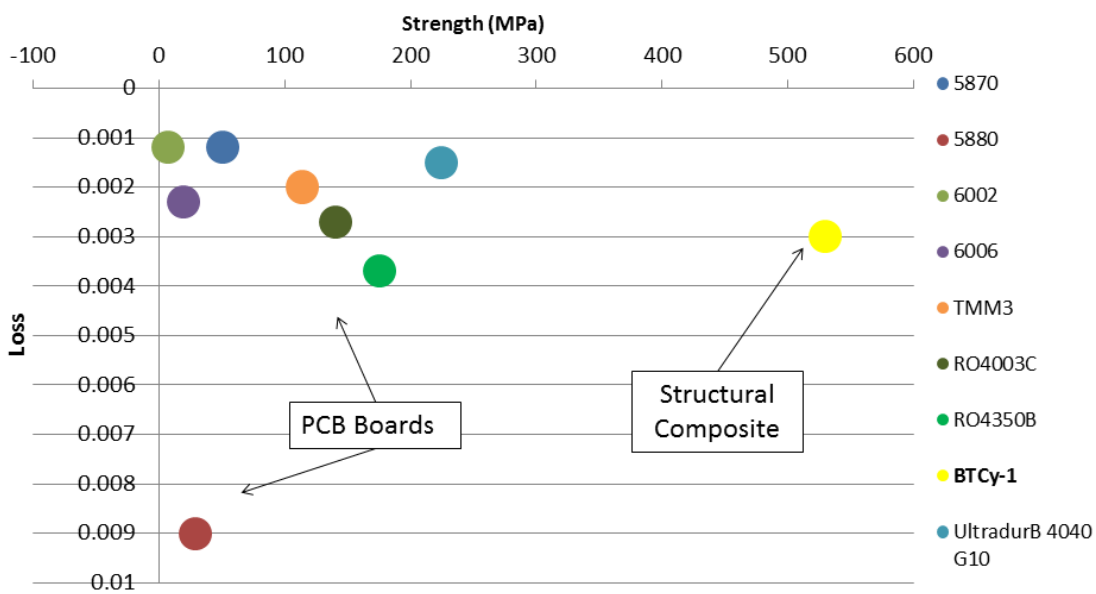

Figure A.1: Printed Circuit Board Materials and Composite System, Signal Loss and Tensile Strength

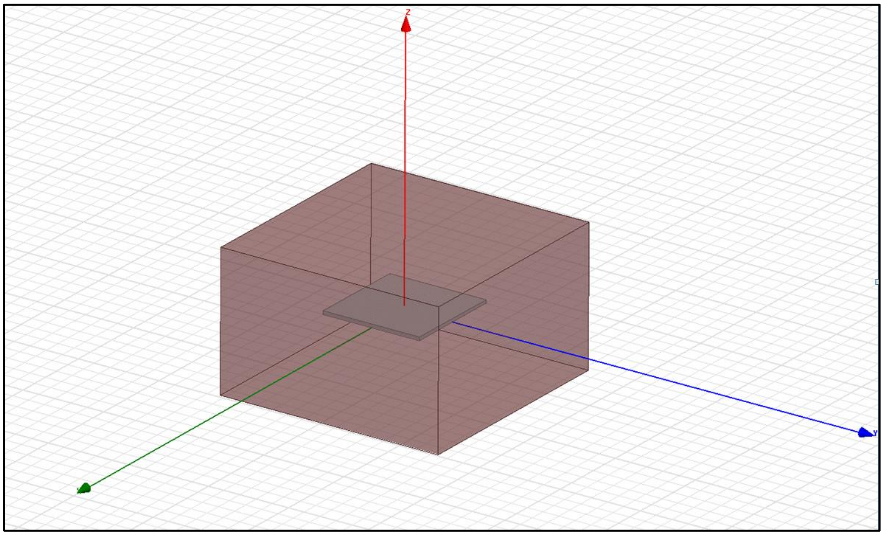

Figure A.2: HFSS Model FSS Unit Cell

FSS models were first simulated using the software HFSS developed by Ansys®. They were simulated as though they were part of a composite laminate stack much like the panels which where mechanically tested earlier. Figure A.2 shows an example of a unit cell model which would then be arranged periodically to model the entire FSS panel. Some alterations had to be made to the model after FSS fabrication as subtle changes in the thickness of the composite affected the dielectric properties of the FSS. All FSS panels made were measured in the anechoic chamber before mechanical testing.

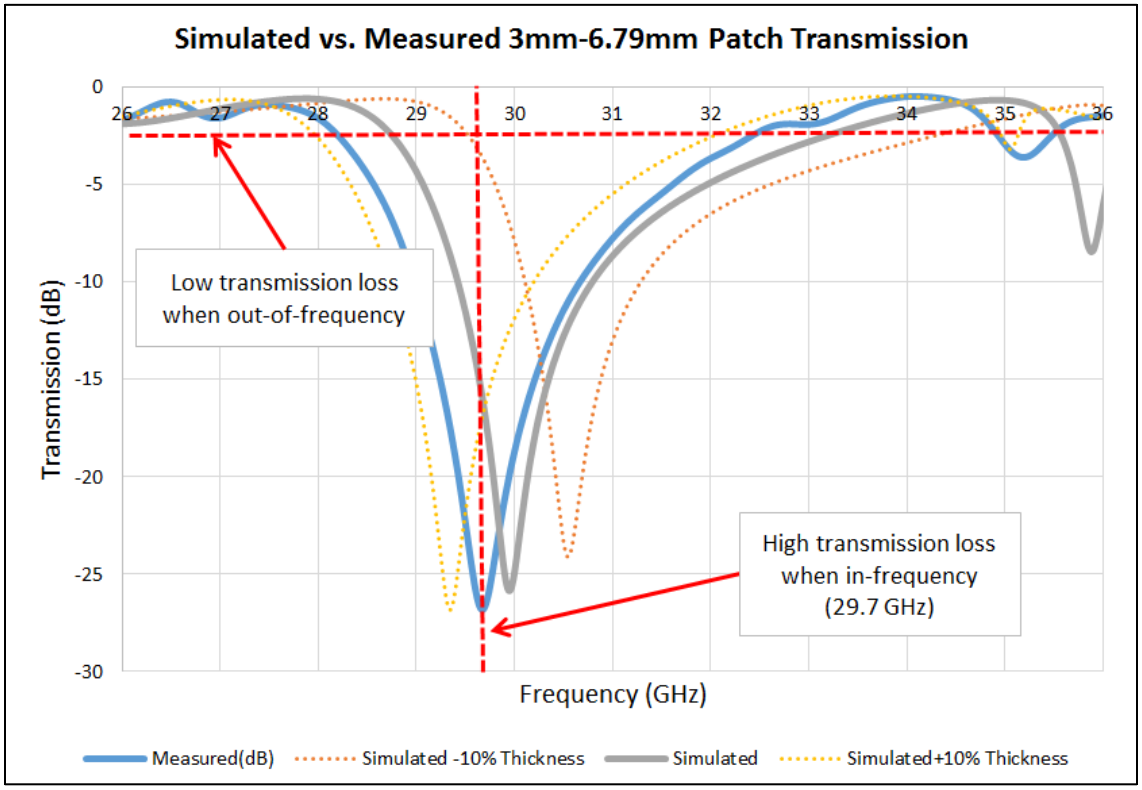

Figure A.3: HFSS Simulation Result of Transmission Varying Frequency

An example of the simulation and measurement results can be seen in Figure A.3. Here the transmission through the FSS panel was measured as a function of the frequency. As mentioned before the FSS has very low loss when out-of-frequency but much higher loss when in-frequency. For this example that happens to be at 29.7 GHz where the FSS panel acts much like a ground plane blocking the microwave signal. There was a slight deviation between the model and the actual measured FSS made. This was due to variation in the thickness of the composite laminate on either side of the FSS layer. More accurate models could be made knowing the statistics of the thickness variation in the final laminates although this is not the focus of the paper.

The actual pattern geometry, size and spacing, were chosen through iterating designs in HFSS. First, patch spacings were calculated such that when each sample was cut, there would be proper alignment of the patches on each sample. This was done assuming cuts were made with a 1.78 mm (0.07 inch) blade width and corresponds to the number of patches that can fit in a 2.54 cm (1 inch) square. The results of these simulations can be seen in Figure A.4. Resonant frequencies were recorded as well as the amount of loss at those frequencies. The cells marked in red were ruled out as they did not behave well as FSS's. This gave us a grid of applicable configurations to choose from shown in blue and green. The graphs below show the actual simulation output with frequency sweep.

Spacing (mm)			Resonant Freq. Size (mm) 1	2	3	4	5	6	7	8	9	10
	2x2	13.6	37.39	21.00	27.07	19.83	19.52	28.17	18.31	25.60	22.98	22.51
		11	33.14	31.68	23.55	23.19	22.51	21.49	20.20	19.52	21.72	24.08
	3x3	9.07	29.68	28.01	27.22	26.49	25.02	19.68	19.21	27.64	26.17	
	4x4	6.79	27.90	25.28	23.61	23.92	26.38	33.25				
	5x5	5.44	32.80	28.37	28.59	31.83	38.91					

Spacing (mm)			Loss at Resonant Freq. Size (mm) 1	2	3	4	5	6	7	8	9	10
	2x2	13.6	-1.40	-4.67	-9.69	-14.38	-16.47	-18.00	-18.09	-23.05	-7.18	-22.29
		11	-0.70	-4.32	-11.21	-14.87	-16.91	-19.76	-25.43	-27.30	-61.46	-56.68
	3x3	9.07	-1.10	-10.40	-21.49	-29.85	-31.61	-40.96	-32.68	-46.86	-30.24	
	4x4	6.79	-2.12	-14.06	-26.72	-34.35	-35.30	-42.10				
	5x5	5.44	-2.54	-19.03	-30.62	-34.19	-36.01					

Lengend
Good FSS
Bad FSS

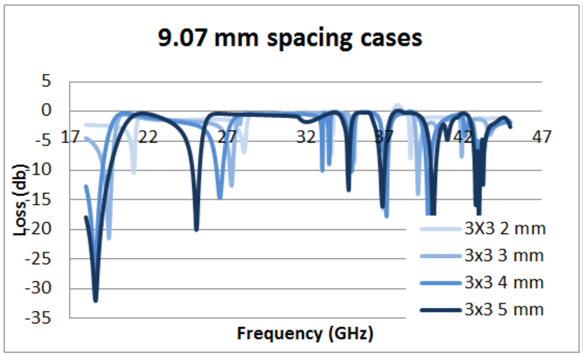

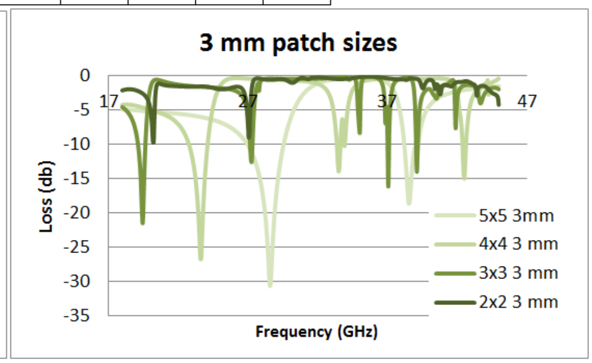

Figure A.4: FSS Simulation Sweep Results